Title: The Basal Ciliary but not Cytosol PKA Specifically Regulates HH Pathway Downstream of Smoothened

Hongyu Zhang[1], Zhuoya Huang[1], Shujing Chen[1], Guangxin Chen[1], Jin Ben[2], Philip Ingham[3,4], Zhonghua Zhao[1,4]

1. The key laboratory of Medical Molecular Cell Biology of Shanxi Province, Institute of biomedical sciences; The key laboratory of Chemical Biology and Molecular Engineering of Ministry of Education, School of Life Science, Shanxi University, Taiyuan, China

2.School of Life Science, Yunnan University, Kunming China.

3. Department of Life Sciences and Milner Centre for Evolution, University of Bath, Bath, UK.

4. Corresponding author: Zhonghua Zhao, zhzhao@sxu.edu.cn; Philip Ingham, pwi20@bath.ac.uk

Running title: The Basal Ciliary PKA specifically regulates HH pathway

Abstract

Effectors of the vertebrate Hedgehog (HH) signaling pathway are organized through primary cilia (PC) that grow and retract in lockstep with the cell cycle in response to extracellular signals. Protein kinase A (PKA), a kinase with ubiquitous distribution in most cells, functions as a specific negative regulator of the HH pathway. Its functional specificity in the HH pathway has been suggested to be controlled by cAMP in the PC. However, the regulation of PKA and its functions in PC is still poorly elucidated, partially due to the lack of observation of PKA localization in PC and inconsistency in the fluctuation of ciliary cAMP with HH pathway activity. Herein, we have developed an effective biosensor for monitoring real-time PKA activity in the PC of both cultured cells and zebrafish embryos, using a ciliary specific localized FRET-based A-kinase activity probe (Nphp3N-AKAR2-CR). Although the PKA catalytic subunit (PKA-C) was not observed in PC, ciliary PKA basal activity in cells was detected by Nphp3N-AKAR2-CR. Notably, its activity was modestly increased both by inhibition and activation of the HH pathway at the level of Smoothened (Smo). In addition, we have found that only ciliary-targeted PKA and not cytosolic PKA, can specifically modulate the HH pathway, even when the integrity of the PC is disrupted. Our results suggest that a basal level of PKA activity in the PC maintains the HH pathway in the OFF state and that PKA mediated inhibition is countered by changes in GLI concentration in the PC.

Introduction

The HH signaling pathway is conserved from cnidaria to vertebrates, playing critical roles in embryonic development and adult tissue and metabolic homeostasis (Ingham et al, 2011). Abnormal HH pathway activity results in multiple developmental defects and is also implicated in the onset and progression of various malignant cancers (Barakat et al., 2010; Scales and Sauvage, 2009; Taipale and Beachy, 2001). The mechanism of HH signal transduction has been extensively studied in vertebrate systems, including mice, zebrafish and cultured cells, as well as invertebrates, especially *Drosophila,* in which it was first characterized. Most of the core components of the pathway are shared between phyla and have highly similar mechanisms controlling the transduction of the HH signal. However, the process is more complex in vertebrates, especially due to its dependence on the primary cilium (PC), a highly specialized subcellular compartment.

Cilia are microtubule-skeleton organelles that protrude from the cell surface and are present in nearly all vertebrate cells. They are categorized into motile and non-motile cilia according to their structure and function. The PC are non-motile and function primarily as sensors, detecting both intracellular and extracellular signals and precisely regulating intracellular signal transduction, with a solitary PC found in each cell (Schou et al., 2015; Derderian et al., 2023). The proteins that can enter the PC are highly selected and accurately controlled. The PC is implicated in the functioning of several signaling pathways including HH, Notch, NF-κB, and PDGF, (Ingham, 2022; Schneider et al., 2005; Grisanti et al., 2016; Christensen et al., 2012). Amongst these, the dependence of the HH pathway on the PC is perhaps the best characterized. Most of the key HH signaling components, namely Patched1 (PTCH), Smoothened (SMO), Glioma-associated-oncogene (GLI), Kinesin like member 7 (KIF7), Suppressor of Fused (SUFU), exit from or accumulate in the PC during pathway activation and

disruption of PC structure or transport mechanism causes perturbation of HH activity. A major event in PC regulation of HH pathway activity is the divergent phosphorylation of the GLI proteins leading to their activation or suppression (Rimkus et al., 2016; Dilower et al., 2023). Protein Kinase A (PKA), one of the key negative regulators of the HH pathway, is considered to be the critical kinase for phosphorylating GLI and promoting its cleavage to a repressor form, thereby inhibiting HH pathway target gene activation (Concordet et al 1996; Johnson et al 1995; Lepage et al., 1995; Li et al., 1995; Hammerschmidt et al., 1996; Robbins et al., 1997; Zhang et al., 2015).

The PKA holoenzyme is a heterotetramer composed of two catalytic subunits (PKA-C) and two regulatory subunits (PKA-R), that are ubiquitously expressed and involved in many intracellular signaling pathways mediating numerous physiological processes including cell proliferation, metabolism, memory formation and muscle function (Rosenberg et al., 2002; Bollen et al., 2014; Torella et al., 2009). The localization of PKA to specific subcellular compartments is crucial for its diverse signaling functions (Scott and Pawson, 2009; Pawson, 2004). The activity of PKA is controlled by cyclic adenosine monophosphate (cAMP), which binds directly to the PKA-R, releasing the active PKA-C (Torres-Quesada et al., 2017). Generally, cAMP level is regulated by Adenylyl Cyclases (ACs) in a G-protein dependent manner, whereby the ACs are either activated or inhibited by the $G\alpha_s$ or $G\alpha_i$ subunit, respectively, in response to G Protein-Coupled Receptor (GPCR) activation. In the HH pathway, SMO, an F-family GPCR, has been hypothesized to inhibit PKA activity by directly sequestering the PKA-C subunit or activating $G\alpha_i$, while GPR161 has been suggested to increase the PKA activity through $G\alpha_s$ (Ogden et al., 2008; DeCamp et al., 2000; Shen et al., 2013; Mukhopadhyay et al., 2013; Walker et al., 2024). Both GPCRs are localized to the PC and show opposing ciliary accumulation in response to HH signaling, implying that PKA may regulate HH pathway activity in a PC dependent manner. However, although the ciliary

localization of the PKA-C subunit has been inferred from proteomics analysis, only the PKA-R subunit and not the PKA-C has been directly visualized in the PC (Mick et al., 2015). Moreover, cAMP levels are slightly elevated in the PC when SMO, the obligate transducer of HH signaling, is either activated or inhibited, confounding the association between ciliary PKA and HH pathway activity.

In this study, we have established a visualization tool for the real-time dynamic monitoring of PKA in PC, by targeting the FRET-based A-kinase activity probe (AKAR2) to the PC using the N-terminal region of zebrafish Nephrocystin-3 (Nphp3) (Zhang et al, 2022). This tool enables stable and dynamic monitoring of PKA activity in PC of both cultured cells and intact embryos. Surprisingly, we found that PKA activity in the PC was not changed following perturbation of the HH pathway at the level of SMO. In addition, Nphp3N has been utilized to deliver different PKA variants specifically to either the PC or the cytoplasm in both cells and embryos, thus modulating the PKA activity levels inside and outside the cilium. Taken together, our findings suggest that a basal level of PC-localized, but not cytoplasmic, PKA specifically regulates HH signal transduction in cells.

Results

1. AKAR2 functions as an active PKA probe in NIH3T3 cell

The AKAR2-CR biosensor is a FRET-based Protein A-kinase (PKA) activity probe developed to monitor PKA activity in HeLa cells and HEK-293T cells (Ni et al., 2006; Allen and Zhang, 2006). It is composed of a fusion protein consisting of a phosphor-peptide binding domain, a Forkhead-associated domain (FHA1), and a consensus region of PKA substrates sandwiched between a donor fluorophore (Clover) and an acceptor fluorophore (mRuby2). In the absence of PKA activity, AKAR2-CR maintains a straight structure such that the Clover and the mRuby2 fluorophores are separated, leading to low FRET

efficiency. When the central substrate is phosphorylated by PKA-C, the AKAR2-CR folds, bringing the two fluorophores into close enough proximity for FRET to occur efficiently. Thus, AKAR2-CR can accurately report PKA activity within cells (Fig. S1A).

Because PC are more robust and easier to detect in NIH 3T3 cells, we first confirmed that the reporter functions in these cells. By transfecting *pCS2(+)-AKAR2-CR* construct into NIH 3T3 cells, AKAR2-CR was expressed and evenly distributed in such cells (Fig. S1B and C). Consistent with the FRET assay in HeLa cells, the AKAR2-CR sensor showed an increase of the Clover fluorescence intensity following the bleaching of mRuby2 when the cells were treated with forskolin, which activates PKA by upregulating AC activity (Fig. S1F). The significant increase in relative FRET efficiency indicated that the AKAR2-CR probe is a useful live-cell biosensor to monitor the PKA activity changes in NIH3T3 cells (Fig. S1D and E).

Next, we examined whether AKAR2-CR could be used to monitor ciliary PKA activity. To target the reporter specifically into the PC of NIH3T3 cells, Nphp3N, which has been shown to be a specific and efficient ciliary targeting peptide (CTP), was fused to the N terminus of AKAR2-CR. When introduced into NIH3T3 cells, the Nphp3N-AKAR2-CR was normally expressed and specifically localized to the PC (Fig. 1A and B), as indicated by the overlap of Clover and mRuby2 signals with immunofluorescence (IF) staining of the acetylated tubulin, a cilia marker (Fig. 1A). When transfected cells were stimulated with forskolin, the FRET efficiency in the PC increased by ~9% (Fig. 1C and D), as indicated by an increase in Clover signal intensity in the PC following mRuby2 bleaching (Fig. 1E). This demonstrates that the Nphp3N-AKAR2-CR biosensor can accurately and efficiently report PKA activity in the PC of the NIH3T3 cells.

The PKA biosensor was next used to investigate PKA activity in the cytoplasm or the PC during HH signal transduction. Activation or inhibition of

the HH pathway was achieved by treating cells with the SMO agonist, SAG, or its antagonist, Cyclopamine (CycA), respectively. Cytosolic PKA activity was slightly increased after treating with either SAG or CycA, as indicated by enhancement of the FRET efficacy of the AKAR2-CR in the cytoplasm (Fig. S1D and E). However, no obvious difference in cytosolic PKA activity between the two treatments was observed. Contrary to expectation, the ciliary PKA activity showed a very slight but non-significant increase following treatment with either SAG or CycA (Fig. 1C and D), with no differences between these two treatments.

2. The Nphp3N-AKAR2-CR can report ciliary PKA activity in living organisms

The ease of visualization of early embryonic stages in zebrafish together with robust readouts for cilia and HH pathway activity makes it a good model for investigating the role of PKA in HH signaling in vivo. Transient expression of the Nphp3N-AKAR2-CR in zebrafish embryos showed that it localizes specifically in the PC as in NIH3T3 cells (Fig. 2A). However, the levels of expression varied between cells. To overcome this variability, we generated a stable transgenic line in which Nphp3N-AKAR2-CR is ubiquitously expressed throughout the embryo. A *Tol2* transgene carrying *nphp3N-AKAR2-CR* driven by the *β-actin* promoter was constructed and introduced by microinjection into wild-type one-cell stage embryos (Fig. 2B) (Higashijima et al., 1997). Heritable carriers were identified by fluorescence microscopy and four lines were obtained. The line with the strongest green and red fluorescence, designated Tg (*β-actin*:*nphp3N-AKAR2-CR*)^{sx1002} (*sx1002* hereafter), was employed for all subsequent analyses. The *sx1002* fish develop normally and are fertile. Nearly all the PC of different cells analyzed in *sx1002* embryos exhibited Clover and mRuby2 signal simultaneously (Fig 2C), suggesting that the Nphp3N-AKAR2-CR fusion protein maintained stable and persistent localization within the PC. No obvious defects in the structure or distribution of the cilia were observed in

the transgenic embryos indicating that Nphp3N-AKAR2-CR expression does not affect PC integrity.

We first used the *sx1002* line to investigate whether activating or inhibiting SMO modulates PKA activity in the PC of living embryos. Transgenic embryos were injected with *shh* mRNA or treated with CycA, and the relative FRET efficiency was assayed as described. No significant change in PKA activity in the PC was detected in either case (Fig 2D and 2F). The effect of each treatment on HH pathway activity was confirmed by staining embryos for Prox1a, a marker of slow twitch muscle specification that is mediated by HH signaling. (Fig. 2E)

To determine whether changes in PKA activity can be detected in the *sx1002* embryos, we next microinjected them with mRNA encoding either the constitutively active PKA (cPKA) or dominant negative PKA (dnPKA) (Concordet et al 1996; Hammerschmidt et al., 1996), and the relative FRET efficiency was examined in each case. Injection of the dnPKA mRNA led to a significant decrease in the FRET efficiency in the PC compared to the controls (Fig. 2C, D and F), indicating that the *sx1002* transgenic line can accurately reports changes in PKA activity in the PC. Surprisingly, however, no significant change in the dynamic range of FRET was observed in embryos injected with cPKA mRNA, (Fig. 2D and F). We speculated that this could be due to the injected cPKA not entering the PC. To test this hypothesis, the subcellular localization of cPKA and dnPKA was visualized by expressing cPKA-eGFP and dnPKA-eGFP in zebrafish embryos. Subcellular localization of the fusion proteins examined by IF staining of 18hpf embryos revealed that cPKA-eGFP was mainly localized in the cytoplasm, whereas the dnPKA-eGFP was observed both in the cytoplasm and the PC (Fig. S2), indicating that the exogenous dnPKA and cPKA proteins are differentially localized in zebrafish embryos.

3. Specific delivery of functional PKA to the primary cilia.

Ciliary localization of the PKA catalytic subunit has not previously been observed. Given the observed divergence of the subcellular localization of the cPKA and dnPKA, we proposed that the Nphp3N CTP fused to the N terminal of cPKA and dnPKA may deliver these two functional proteins into the PC. Although the Nphp3N could precisely drive the AKAR2 and other fluorescent proteins into the PC in both cultured cells and zebrafish embryos, the Nphp3N-cPKA and dnPKA fusions did not specifically localize to the PC but were also present in the cytoplasm when transiently expressed in cells and zebrafish embryos (Fig. S3). We speculated that the proximity of the Nphp3N peptide and PKA resulted in spatial constraints, which in turn caused the misfolding of the proteins, and thus potentially interfered with their original localization and function. To circumvent this, a hydrophilic flexible linker peptide $(GGGGS)_2$ was inserted to increase the distance between Nphp3N CTP and the PKA functional domain and thus improve the proper folding of each domain. These linker-modified versions of the Nphp3N-cPKA and dnPKA fusions both localized efficiently and specifically in PC, with the PC efficiencies up to 82.5% and 89.5% respectively following transient expression (Fig. 4A, 4B, 4I and 4J). The Glycine of the second residue of Nphp3N is critical for its ciliary targeting function, and the G2A mutation impairs its ciliary localization property (Zhang et al., 2022). Consistently, the localization of the Nphp3N-G2A-cPKA and dnPKA fusion proteins were observed only in the cytoplasm, providing a good opportunity for examining the cilia- and cyto- PKA function separately (Fig. 4A, 4B, and S4).

Specific delivery of dnPKA to the cilia and cytoplasm respectively in zebrafish embryos using two variants of the Ras-related protein RAB23, RAB23-Q68L and RAB23-S23N, has previously been reported (Truong et al., 2021). To compare the efficiency of the two ciliary delivery systems, the RAB23-Q68L-cPKA/dnPKA and RAB23-S23N-cPKA/dnPKA were generated and their expression and subcellular localization examined by microinjection of

mRNA into zebrafish embryos. The cPKA/dnPKA-eGFP fused with RAB23 variants were expressed at much lower levels than the same proteins fused with Nphp3N and its variants at 6 hours post injection (hpi) and later stages (Fig. S5). Similarly, the efficiency of ciliary localization of the cPKA/dnPKA-eGFP fused to RAB23-Q68L was much lower than that driven by Nphp3N (Fig. 4E, 4F, 4I, 4J and S6), indicating that the Nphp3N is a superior system for delivering proteins to the PC.

To investigate the function of ciliary localized Nphp3N-cPKA/dnPKA, their mRNAs were injected into embryos of the *sx1002* PKA biosensor line. As expected, the Cilia-cPKA or dnPKA showed an increase or decrease, respectively, in the FRET efficiency of ciliary AKAR2 (Fig. 3A, B and C). By contrast, no change in FRET was detected following injection of the Cyto-cPKA/dnPKA mRNAs compared to the control group (Fig. 3A, B and C). Thus, we have successfully developed an efficient method for specifically delivering functional proteins to cilia using Nphp3N CTP.

4. Ciliary PKA effectively regulates HH pathway activity

The localization of PKA to specific subcellular compartments is crucial for its diverse signaling functions (Scott and Pawson, 2009; Pawson, 2004). Although the RI subunits of PKA have been reported as being localized in PC (Mick et al., 2015), there is no direct evidence to show that the PKA-C resides in the PC, raising the question of where PKA regulates HH signal transduction. The method of ciliary targeting of functional PKA we have established provided an opportunity to analyze the relative contributions of cilia-PKA and cyto-PKA to vertebrate HH pathway activity (Fig. 5A) .

When the cPKA, Cilia-cPKA (Nphp3N-cPKA) or Cyto-cPKA (Nphp3N-G2A-cPKA) were introduced into *sx1005* embryos by microinjection, each protein was normally expressed at 18hpf, as indicated by Western blot, and localized to the cilia and cytoplasm respectively (Fig. 4A, 4B and 4C). To

assay HH pathway activity, we used an En2a::eGFP reporter line, Tg(*en2a:eGFP*)^{sx1005} (*sx1005*; see Material and Methods) and stained the embryos for Prox1a protein, as previously described (Maurya et al 2011).

Compared with wild type embryos, although the cPKA and Cyto-cPKA injected embryos showed certain abnormalities, the numbers of Prox1a+ cells and En2a+ cells as indicated by En2a:GFP were similar to the wild-type embryos, indicating the Cyto-cPKA has little effect on HH pathway activity. By contrast, however, the Cilia-cPKA injected embryos lacked all Prox1a+ and En2a+ cells in myotome, demonstrating that the Cilia-cPKA specifically inhibits HH signal transduction (Fig. 5B and 5D). Additionally, analysis by in situ hybridization revealed that only Cilia-cPKA resulted in depletion of the expression of HH pathway target genes, such as *ptch2*, *oligo2* and *nkx2.2*, whereas cPKA and Cyto-cPKA had no effect on the expression levels of these genes (Fig. 5C).

By contrast, injection of either dnPKA or Cilia-dnPKA mRNA into embryos resulted in a significant increase of the En2a+ and Prox1a+ muscle cells in *sx1005* (Fig. 5B and 5D). Consistently, *ptch2*, *oligo2* and *nkx2.2* were all ectopically expressed in these embryos (Fig. 5C). By contrast, embryos injected with the Cyto-dnPKA (Nphp3N-G2A-dnPKA), showed normal expression of HH-pathway target genes and similar numbers of the En2a+ and Prox1a+ cells in myotome as in wild-type embryos. Taken with the finding that the untagged dnPKA can localize to cilia (Fig. 4B), this suggests that the HH signaling pathway is activated only by the inhibition of PKA in the PC.

The effects of cPKA and dnPKA fused with RAB23 Q68L and S23N, were also examined. Both the RAB23-Q68L-cPKA and -dnPKA showed little if any effect on HH activity, as the numbers of the En2a+ and Prox1a+ cells in myotome were similar to those in wild-type embryos when these two fusion proteins were expressed in embryos (Fig. 5F). This could be due to the inefficient cilia delivery and low expression of these fusion proteins as

described above. Consistently, with the same amount (50μg) of the total protein used for Western blot assay, the RAB23-Q68L-cPKA and dnPKA could hardly be detected whereas the Nphp3N-cPKA and dnPKA bands were overexposed (Fig S5B). This demonstrates that a level of ciliary PKA above a certain threshold is required to regulate HH signal transduction.

The detection of PKA-R but not PKA-C in the PC by immunofluorescence suggests that the low level of PKA-C must be strictly controlled. If this is the case, increasing the levels of PKA-C in the PC should have a similar effect as the Cilia-cPKA. To test this hypothesis, the Nphp3N-PKA-C mRNA was injected into embryos. Like the Cilia-cPKA, the protein localized to the PC (Fig. 5I) and efficiently suppressed HH activity, as shown by the depletion of both Prox1a+ and En2a+ cells in the myotome (Fig. 5H and 5J). In contrast, the untagged PKA-C, which was only observed in the cytoplasm, had no effect on HH activity (Fig. 5H and 5J).

In vertebrates, the dependence of HH signaling upon the PC, is reflected by a mild upregulation of HH pathway activity caused by PC aberrations in mouse and zebrafish embryos (Huangfu et al., 2003; Bazzi et al., 2014; Davey et al., 2006). Our findings imply that HH signaling may require a basal level of PKA-C activity in the PC to function as a ciliary effector, responding to fluctuations in signaling molecules within distinct subcellular locales. Thus, we hypothesize that in the absence of the PC, the cyto-PKA would be functional in regulating HH pathway in the same way as the cilia-PKA. To test this, the PC was disrupted in zebrafish embryos by knockdown of the *dzip1* (DAZ Interacting Zinc Finger Protein 1), which has been shown to be critical for primary ciliogenesis and HH signal transduction (Wolff et al., 2004; Kim et al 2010; Tay et al 2010; Chen et al., 2024). As previously shown (Tay et al., 2010), knockdown of Dzip1 by splicing morpholino resulted in a reduction of the number of PCs in paraxial mesodermal cells (Fig. 6B) and ectopic expansion of En2a expression, indicated by the expansion of eGFP fluorescence in *sx1005*

embryos (Fig. 6A). Next, we verified that in the absence of cilia is where PKA regulates the HH pathway. All injected mRNAs were proved to be expressed by Western Blot (Fig. 6D). Unexpectedly, however, co-injection of the *dzip1* morpholino together with either Cyto-cPKA or Cyto-dnPKA led to the same abnormal HH activation as in *dzip1* morphants (Fig. 6A and C), whereas co-injection of the *dzip1* morpholino with either Cilia-cPKA or Cilia-dnPKA resulted in the same phenotype as the Cilia-cPKA/dnPKA (Fig. 6A and C). Notably, a few cilia remained following knockdown of Dzip1, and they were all positive for the Cilia-cPKA or dnPKA (Fig. 6B). This suggests that the extraciliary PKA or non-ciliary associated PKA has no regulative role in HH signaling even when the PC is disrupted.

5. Control of the downstream HH signal transduction by ciliary PKA

PKA modulates HH signaling both through phosphorylation of GLI transcription factors and of SMO, the obligate transducer of the HH signal (Tempe et al., 2006; Pan et al., 2009; Niewiadomski et al., 2014). To investigate the level at which cilia-PKA functions, the activation and subcellular localization of SMO and GLI were assayed upon introduction of cilia-cPKA/dnPKA together with perturbation of the HH pathway at different levels. Co-injection of SHH and Cilia-cPKA mRNA into *sx1005* embryos resulted in the loss of expression of both eGFP and Prox1a in the myotome, the same phenotype resulting from injection of Cilia-cPKA alone (Fig. 7A and B). By contrast, embryos injected with Cilia-dnPKA mRNA and treated with CycA, exhibited ectopic expression of eGFP and Prox1a in the myotome, indicative of ectopic activation of the HH pathway (Fig. 7A and B).

Recent studies have shown that phosphorylation of the C-terminal domain of SMO by GRK2 results in its binding and sequestering PKA-C (Walker et al., 2024). SMO is reported to rapidly turn over in the PC at the basal state, and its retention and accumulation in the PC is a key event in its activation. To test

whether cilia-PKA is related to the accumulation of SMO in the PC, the localization of SMO was examined in NIH3T3 cells in the presence of the Cilia-cPKA or dnPKA. Notably, the expression of Cilia-cPKA/dnPKA did not affect the basal level of SMO within PCs (Fig. 7D and E). Similarly, the accumulation of SMO in the PC caused by SAG treatment was not perturbed by expressing Nphp3N-cPKA in these cells, while expression of the Nphp3N-dnPKA, which can fully activate the HH pathway did not increase the PC localization of SMO (Fig. 7D and E).

KIF7 is one of the key components that regulates HH pathway activity downstream of SMO; in both mouse and zebrafish *kif7*$^{-/-}$;*smo*$^{-/-}$ double knockout mutants present a HH gain of function phenotype similar to that of the *kif7*$^{-/-}$ single mutant (Endoh-Yamagami et al., 2009; Maurya et al 2013). To validate the epistasis of cilia-PKA in the HH pathway, different PKA variants were expressed in *kif7*$^{-/-}$ null mutant zebrafish. The localisation of the Cilia-cPKA/dnPKA to the PC and of the Cyto-cPKA/dnPKA to the cytoplasm was unaffected in the absence of KIF7 (Fig. 8B and D). Expression of Cilia-cPKA was sufficient to suppress ectopic En2a:GFP expression in *kif7* mutant embryos (Fig. 8A and C), indicating that PKA acts downstream of KIF7 to attenuate pathway activity.

In addition, further validation was performed on cellular models. First, the subcellular localization of Cilia-cPKA/dnPKA and Cyto-cPKA/dnPKA in NIH3T3 was verified. Consistent with the results in the zebrafish model, the proteins guided by Nphp3N were all localized in the PC, whereas the protein carried by Nphp3N-G2A was widely expressed in the cytoplasm (Fig. S7). Considering the limitation of transfection efficiency, Nphp3N-cPKA/dnPKA stably expressing cell lines were created using a lentiviral system. Nphp3N-cPKA and Nphp3N-dnPKA stable cell lines were treated with SAG and CycA, respectively. Western blot analysis showed that even in the presence of SAG-mediated activation, Cilia-cPKA could increase the processing of GLI3,

resulting in a corresponding increase in GLI3R levels. In contrast, CycA could not inhibit the reduction of GLI3R protein induced by Cilia-dnPKA (Fig. 7C). In summary, although an effect of cilia-PKA on SMO cannot be ruled out, the major role of cilia-PKA in regulating HH pathway occurs downstream of SMO.

Discussion

Primary cilia (PC) play important roles in regulating vertebrate HH signal transduction and PKA activity in the PC is considered to be a critical aspect of the requirement for the PC in this signaling cascade; however, the precise details of the processes supported by the PC are still unclear. Here, we have developed a new method for monitoring PKA activity in the PC, both in tissue culture and in living embryos. Using this tool, we found that PKA activity in the PC was not changed following perturbation of the HH pathway at the level of SMO. However, when PKA activity was specifically modified by directly delivering cPKA or dnPKA to the PC, the changes in its activity could dramatically activate or suppress HH signal transduction downstream of the SMO. The regulation of the HH pathway by PKA is absolutely dependent on the PC, whereas cytosolic PKA has no effect on HH pathway activity in vertebrate cells. Our study provides a new perspective on the mechanism of vertebrate HH pathway activity by PKA. The tool for delivering functional proteins, including cPKA and dnPKA, to the PC will enable future studies of protein function in the PC and new options for the development of therapeutics targeting the PC and HH pathway related human diseases.

Compartmentalized activity underpins the precise regulation of key cellular processes mediated by PKA (Li et al., 2013; Wong et al., 2004; Taylor et al., 2012). Tracking the activity of PKA in living cells enhances our understanding of this regulation. To achieve this, two strategies could be adopted: measuring either the cAMP concentration or PKA activity directly. So far, only tools for monitoring cAMP level in PC by Arl13b-H187 or 5HT6-mCherry-cADDis have

been reported (Tewson et al., 2016; Moore et al., 2016; Jiang et al., 2019). Although the major pathway activated by cAMP is PKA-dependent, cAMP can also activate Epac and cyclic nucleotide-gated (CGN) ion channels directly, independently of PKA (Beavo and Brunton, 2002). Thus, cAMP level is not synonymous with PKA activity. By using the AKAR2-CR probe, in which a FRET signal is produced by the conformational change caused by phosphorylation of the PKA substrate peptide, we were able to assay directly the exact level of PKA activity. For specific delivery of the PKA biosensor to the PC, instead of the commonly used Arl13b or 5HT-6, we used the Nphp3N CTP peptide. This design was more suitable for the specific study of the PC since the Nphp3N is much smaller than Arl13b and 5HT-6 and has been confirmed to have little effect on PC integrity (Zhang et al., 2022). Accordingly, we generated a stable zebrafish transgenic line ubiquitously expressing the Nphp3N-AKAR2-CR fusion protein, allowing monitoring of PKA activity at the individual PC level. This line will facilitate further studies on PKA in the PC in living animals.

PKA has been found to be a major player in HH signal transduction. However, it is still controversial whether PKA regulation of the vertebrate HH pathway is absolutely dependent on the PC. This is partly because there is as yet no direct evidence of the presence of the PKA-C in the PC, although the basal cilia PKA level was reported higher than the cytosol PKA activity when the compartmented PKA activity was examined by 5HT6-AKAR4 (Moore et al., 2016). The 5HT6 has been widely used for ciliary targeting of non-ciliary proteins; however, its large size and its native function as a GPCR in cilia give grounds for caution in drawing conclusions based on its use. Moreover, rather than localization to the PC, PKA was also reported to localize specifically at the basal body, which suggested that this basal body localization of PKA was critical for its role in the HH pathway (Tuson et al., 2011; Peng et al., 2021). Recently, a faint signal of PKA-C sequestered by activated SMO was reported

to be observed in the PC when the HH pathway was activated by SAG after 6 hours (Walker et al., 2024). However, in our assay, we still failed to detect the PC localization of PKA-C directly either in NIH3T3 or zebrafish embryos under different statuses of HH pathway activity, or was the basal body localization observed. The failure of direct detection of the PKA-C by immunofluorescent staining could be either because the translocation of the PKA within the PC is too rapid to be captured by confocal microscopy, or because the basal PKA-C in the PC is below the limit of detection. Nevertheless, our finding that dnPKA and Cilia-dnPKA decrease ciliary PKA activity confirms the presence of a low basal level of PKA-C in the PC. The level must be strictly controlled as we also failed to detect the cPKA within the PC when it was overexpressed. The low basal level of PKA in PC remains constant, as no significant PKA activity change in the PC when perturbing the HH pathway. This is consistent with the observation reported by Jiang et al. when they monitored cAMP level in the PC whilst activating the HH pathway with SAG (Jiang et al., 2019). However, perturbation of ciliary PKA activity at a certain threshold, as shown by Nphp3N-cPKA and dnPKA (but not Rab23-cPKA/dnPKA) did dramatically change the HH pathway activity in our assay, demonstrating that the maintenance of the basal level of ciliary activity is critical for the ON and OFF states of vertebrate HH pathway. Notably, cPKA or dnPKA could regulate the HH pathway only when localized to the PC. However, in the absence of the PC, the cilia-targeted forms of cPKA/dnPKA but not the cytosolic forms are still able to regulate pathway activity. We speculate that in the absence of PC, HH signalosomes can function within a cytosol-localized cilia-related compartment, which could be composed of PC components and related signaling molecules in the cell.

Our finding that PKA activity is unchanged by stimulation or inhibition of Smo activity runs counter to the notion that the cellular response to HH signals is mediated by the regulation of PKA activity. Instead, the catalytic activity of

PKA in PC appears to be maintained at a constant low level; the transcriptional response to HH signaling could thus be achieved by increasing the levels of GLI proteins within the PC such that they escape phosphorylation by the basal PKA activity rather than by modulation of PKA activity itself. Based on these results, we propose a model of the regulation of vertebrate HH pathway by ciliary-localized PKA. In the OFF state, much of the GLI protein is sequestered by SUFU in the cytoplasm and the levels entering the PC, can be efficiently phosphorylated by the basal PKA-C activity. Upon HH pathway activation, there is an increase in the trafficking of GLI into the PC, such that most of the GLIs escape prime phosphorylation by PKA, leading to their dissociation from SUFU and activation. As HH ligand levels fall, movement of GLI into the PC abates and the low level of PKA activity within the PC maintains the HH OFF state by phosphorylating GLI (Fig. 9). How HH controls GLI trafficking into the cilia remains unclear but is thought to be regulated by KIF7 and IFT proteins (Maurya et al., 2013; Ku et al., 2024).

One achievement of our work is that we have established a powerful specific delivery system of the functional protein, especially cPKA and dnPKA to the primary cilium. The smallest cilium target sequence, Nphp3N signal peptide, significantly reduced the adverse effect on cilia caused by the signal peptide, and the linker sequence ensured the proper function of the functional proteins being sent into the PC. This delivery system provides a great opportunity to specifically and efficiently intervene in the PC functions to uncover the mechanism of the PC related cytological processes and signal transductions. To be noted, in our test on zebrafish, we have observed specific regulation role of the Nphp3N-cPKA/dnPKA on the HH pathway. Aberrant activation of the HH pathway has been found to be involved in the occurrence and progression of several tumors, including medulloblastoma, basal cell carcinoma and gastral-intestinal tumors, etc (Berman et al., 2002; Epstein, 2008; Skoda et al., 2018; Walton et al., 2021). And the HH pathway is considered one

of the effective targets for the clinical treatment of these diseases. Compared with the normally used targeted drugs, most of which specifically target on the SMO and show certain adverse side effects and drug resistance, the Nphp3N-cPKA, which shows specific downregulation of the HH pathway, showed a great potential for developing a new reagent against HH-related cancers.

In conclusion, we have established a delivery method that specifically targets cilia, ensuring high efficiency and preserving the functionality of proteins. This strategy effectively counteracts any impacts of other tags on the structure and function of primary cilia. The research on Cilia and Cyto PKA has shown that the activity of the HH pathway can only be efficiently regulated when PKA enters the ciliary shaft. Our results provide new clues for the mechanism of the vertebrate HH signal transduction. And the new PC delivery system allows for precise delivery of multiple proteins and genome-wide tracking of cellular activity, incorporating both temporal and spatial dimensions, as well as dynamic information, to enhance the existing mapping of signal transduction networks.

Material and Methods

Cell Culture of HEK293T and NIH3T3 and Transfection

The HEK293T and NIH3T3 cells, procured from ATCC, were maintained in Dulbecco's Modified Eagle's Medium (DMEM) supplemented with 10% FBS and 10% penicillin-streptomycin, at 37°C with 5% CO2. For ciliogenesis, the cells were initially rinsed with PBS and then subjected to serum starvation by culturing in FBS-free medium for 24 h. For transfection, the Lipofectamine 3000 (Thermo Fisher Scientific, L3000015) or the PEI (MedChemExpress, HY-K2014) were used according to the manufacturer's protocol. To induce or inhibit HH signaling, the cells were plated and treated with either 1 μM SAG (MedChemExpress, HY-12848) or 5 μM cyclopamine (MedChemExpress, 4449-51-8), respectively, and then subjected to the following serum starvation for 24 h prior to collection.

Generation of the stable transgenic cell line

To prepare the lentivirus containing the zNphp3N-cPKA/dnPKA-eGFP, the HEK293T cells were transfected with the plasmids encoding gag-pol (psPAX2), VSV-G (pMD2G), and the plasmid carrying the gene of interest (pLVX-zNphp3N-cPKA/dnPKA-eGFP). Two days post-transfection, the supernatant containing the virus particles was collected and sterilized by filtration through a 0.45 μm filter (Millex-HV, SLHUR33RB) after centrifuged, and stored in -80˚C. The NIH3T3 cells were seeded in 30 mm petri dish with the density at 600,000 cells per dish, and cultured in the mixture of the medium and the collected virus supernatant at 2:1 ratio for three days continuous infection. Then, the puromycin (1-10 μg/ml) was added into the fresh medium for stable cell lines screening.

Zebrafish husbandry

Adult zebrafish of the AB strain, sourced from the China Zebrafish Resource Center, were housed at 28 ℃ on a 14 h light/10 h dark cycle within the zebrafish facility of Shanxi University. Embryos were obtained from natural

mating and grew in E3 medium (5 mM NaCl, 0.17 mM KCl, 0.33 mM $CaCl_2 \cdot 2H_2O$, and 0.33 mM $MgSO_4 \cdot 7H_2O$). The embryos were staged according to the standard developmental staging guidelines (Kimmel et al., 1995).

DNA constructs, RNA synthesis and injection

The transient expression constructs of *pCS2+-nphp3N-AKAR-CR*, *pCS2+-cPKA/dnPKA*, *pCS2+-nphp3N/(G2A)-cPKA/dnPKA-eGFP* , *pCS2+-cPKA/dnPKA-mRAB23(S23N/Q68L)* and the transgenic construct of *pMiniTol2-β-actin-npnp3N-AKAR-CR* and *pMiniTol2-en2a-eGFP* were generated by Gibson assembly. The primers used for cloning are listed in Table S2. The transient expression constructs of *pCS2+-SMO-eGFP*, *pSP64-shh* and *pDB600* were used as described (Maurya et al., 2013; Zhao et al., 2021). The vectors *psPAX2* and *pMD2G* were kindly provided by the lab of Jianguo Li (Institute of Biomedical Sciences, Shanxi University, Taiyuan, China).

For capped mRNA synthesis, the transient expression constructs were linearized by Not I for *pCS2+* constructs, BamH I for *pSP64-shh* and XbaI for *pDB600* plasmid and then purified by Zymogen DNA concentrator. The mRNA was produced using either Sp6 or T3 Invitrogen Ambion mMessagemMachine® Kit according to the promoter in the constructs following the instructions, then purified mRNA were stocked in -80℃ for further use.

For transient expression of the fusion protein in zebrafish embryos, 150 pg of mRNA was injected into one-cell stage embryos.

Generation of zebrafish transgenic lines

To generate the *sx1002* stable transgenic line, the *pMiniTol2-β-actin-npnp3N-AKAR2-CR* construct was co-injected with Tol2 transposase mRNA into one-cell stage embryos. T_0 embryos with strong green and red fluorescence were screened at 24 hpf and inoculated as potential founders. Mature T_0 fish were out-crossed with wild-type, and T_1 offspring with consistent fluorescence were selected as stable transgenic lines.

To create the stable transgenic line Tg(*en2a:eGFP*)^{sx1005} (*sx1005)*, Tol2 transposase mRNA was co-injected into one-cell stage embryos along with the *pMiniTol2-en2a-eGFP* construct (Maurya et al 2011). T_0 embryos with strong green-fluorescence were selected at 24 hpf and inoculated as potential founders. T_1 embryos with steady fluorescence obtained by out crossing of potential founders with wild type were selected as stable transgenic lines.

CRISPR/cas9 genome editing

Guide RNA for CRISPR/cas9 mediated knockout of *kif7* (ENSDARG00000033099) was designed using the ChopChop online server (Montague et al., 2014) and synthesized as described (Wang et al., 2020). Embryos were injected with 1 mg of gRNA and 5 μM of Cas9 protein (NEB, 10128356) at 1-cell stage. Stable *kif7* null allele were screened and identified by PCR using gene specific primers and the following sanger sequencing. The primers used are listed in supplementary Table S2.

FRET imaging

FRET assay was performed as described (Karpova et al., 2003). The NIH3T3 cells and the embryos were prepared. Fluorescence imaging was performed using the LSM 710 confocal inverted microscope (Zeiss). Time stacks of images (512 × 512 pixels, typical field of view 135 μm × 135 μm, 600 Hz scanning frequency) were acquired with a 63× oil immersion objective at room temperature under atmospheric conditions. The pinhole was set at 1AU. The Clover was excited at 458 nm, and its emission was detected in the range 488-514 nm and the mRuby emission was detected in the range >561 nm. Pre-experiments under the emission range of mRuby were carried out to test the bleaching effect. All ROIs are 90% bleached to maximize the bleaching of the acceptor with little or no effect on the donor. At least 2 regions were selected for each field, with one non-target set as the background and the random cell region set as the object. The acquisition of all channel images was set up as a time series of 5 cycles, with bleaching starting after 2 cycles.

For each sample, image time series have been acquired by selecting the field of view populated with more than 40 cells. After acquisition, data have been analyzed through the FRET package of Zen Imaging Software. The ROIs including each cell were selected and the Clover and mRuby fluorescence intensity at different time points before and after bleaching in both acquisition channels were calculated. The relative FRET efficiency was calculated with the following formula: $FRET=100 \times (IF_{Donor, after} - IF_{Donor, before}) / IF_{Donor, after}$. The raw data were then further elaborated with Excel™.

Whole-mount in situ hybridization

The probe of *ptch2*, *olig2*, and *nkx2.2a* for in situ hybridization were prepared as described (Barth and Wilson, 1995; Concordet et al., 1996; Stamataki et al., 2005), and *in situ* hybridization was performed as described (Thisse and Thisse, 2008). Images were captured using Zeiss Imager M2 microscope.

Western blot analysis

Total protein of embryos and culture cells was prepared as described (Maurya et al., 2013; May Et al., 2021). In brief, the embryos were lysed using lysis buffer (20 mM Tris HCl (pH 7.4), 150 mM NaCl, 1% TritonX-100, 10% Glycerol, 2 mM EDTA, and 1 mM PMSF) at the ratio of 1uL lysis buffer per embryo. The culture cells were lysed using RIPA buffer (50 mM Tris-HCl at pH 7.5, 150 mM NaCl, 1% Triton X-100, 1% sodium deoxycholate, 0.1% SDS, 1 mM EDTA, and 1X protease inhibitors). The supernatant was collected after centrifuged at 12, 000 g for 20 min at 4°C, and then was mixed with loading buffer (37.5 mM Tris HCl, pH 7.4; 3% SDS; 0.01% bromophenol blue; 6.25% glycerol; and 100 mM DTT) and boiled for 5 min before PAGE gel assay. Total protein of 40 embryos were separated on 10% acrylamide gel, and then the proteins were transferred onto the PVDF membrane (GE Healthcare Life Science, 10600023). The blocking and antibody incubation were performed accordingly. All antibodies used and their dilution are listed in Table S1. The secondary antibodies labeled by HRP were detected with the super sensitive

ECL substrate kit (Thermo Fisher Scientific, 34580). And the images of the western blot were captured using an infrared imager (GE Healthcare).

Immunofluorescence

Immunofluorescence (IF) staining on embryos was performed as described (Ben et al., 2011). In brief, the embryos were fixed with 4% paraformaldehyde (PFA) at room temperature for 2 h and then stored in -20°C with absolute methanol after dehydration. To proceed IF, the fixed embryos were permeabilized in acetone after rehydrated. Then the embryos were subsequently incubated by blocking buffer (DPBS, 1% BSA, 1% DMSO, 0.5% TritonX-100), primary and secondary antibodies in blocking buffer, and then washed in PBTX (DPBS, 0.5% TritonX-100). The washed embryos were stored in 70% Glycerol/DPBS at 4°C. The antibodies and their titration used in this study were listed in Table S1.

For cell IF staining, the cells were prepared on 14mm coverslips (NEST, 801010), and were fixed with 4% PFA. The IF staining was performed as described (Tsurumi et al., 2019), with the blocking buffer of 1% bovine serum albumin (BSA) in PBS, and antibody in PBS. The antibodies and their titration used in this study were listed in Table S1. The cells on the coverslips were mounted onto microscope slides using the antifade reagent (Beyotime Biotechnology, P0131), after IF staining.

The imaging was conducted using LSM 710 confocal microscope (Zeiss Microsystem, Germany).

Statistics

All experiments were conducted with a minimum of three replicates. Results were displayed as the mean ± standard deviation. *P*-values were determined using one-way ANOVA and t-tests with GraphPad Prism 7.0 software, and the difference with *P*-value less than 0.05 was set as the threshold for statistical significance. All image processing and analysis were performed in ImageJ (Version v1.52i, U.S. National Institutes of Health, Bethesda, Maryland, USA).

Plots and Figures were generated using GraphPad Prism (Version 7.0, GraphPad Software, Inc.) and Adobe Illustrator CS5 (Version v15.0.0, Adobe Systems, Inc.).

Acknowledgement

We are grateful to Michael Lin who kindly deposited the *AKAR2-CR* plasmid used for this study in Addgene, to Changxin Wu for providing the high-level experiment platform. This work was generously supported by National Natural Science Foundation of China (No. 31970738, U21A20389 and No. 81960286), Central Guidance on Local Science and Technology Development Fund of Shanxi Province, (YDZJSX2024D009).

Authors' contributions

H.Z.: data curation, investigation, methodology, project administration, software, validation, writing—original draft; Z.H., S.C. and J.B.: data curation, investigation, methodology, visualization; G.C.: conceptualization, methodology, writing—review and editing; P.W.I.: conceptualization, funding acquisition, resources, supervision, validation, writing—review and editing; Z.Z.: conceptualization, funding acquisition, methodology, project administration, resources, supervision, validation, visualization, writing—review and editing.

All authors gave final approval for publication and agreed to be held accountable for the work performed therein.

Conflict of interest declaration

All authors declare no competing interests.

Reference

[1]. Ingham PW. Hedgehog signaling: a tale of two lipids. Science. 2001 Nov 30;294(5548):1879-81. doi: 10.1126/science.1064115. PMID: 11729305.

[2]. Barakat MT, Humke EW, Scott MP. Learning from Jekyll to control Hyde: Hedgehog signaling in development and cancer. Trends Mol Med. 2010 Aug;16(8):337-48. doi: 10.1016/j.molmed.2010.05.003. Epub 2010 Jun 16.

PMID: 20696410; PMCID: PMC3651907.

[3]. Scales SJ, de Sauvage FJ. Mechanisms of Hedgehog pathway activation in cancer and implications for therapy. Trends Pharmacol Sci. 2009 Jun;30(6):303-12. doi: 10.1016/j.tips.2009.03.007. Epub 2009 May 13. PMID: 19443052.

[4]. Taipale J, Beachy PA. The Hedgehog and Wnt signalling pathways in cancer. Nature. 2001 May 17;411(6835):349-54. doi: 10.1038/35077219. PMID: 11357142.

[5]. Schou KB, Pedersen LB, Christensen ST. Ins and outs of GPCR signaling in primary cilia. EMBO Rep. 2015 Sep;16(9):1099-113. doi: 10.15252/embr.201540530. Epub 2015 Aug 21. PMID: 26297609; PMCID: PMC4576980.

[6]. Derderian C, Canales GI, Reiter JF. Seriously cilia: A tiny organelle illuminates evolution, disease, and intercellular communication. Dev Cell. 2023 Aug 7;58(15):1333-1349. doi: 10.1016/j.devcel.2023.06.013. Epub 2023 Jul 24. PMID: 37490910; PMCID: PMC10880727.

[7]. Ingham PW. Hedgehog signaling. Curr Top Dev Biol. 2022;149:1-58. doi: 10.1016/bs.ctdb.2022.04.003. Epub 2022 May 6. PMID: 35606054.

[8]. Grisanti L, Revenkova E, Gordon RE, Iomini C. Primary cilia maintain corneal epithelial homeostasis by regulation of the Notch signaling pathway. Development. 2016 Jun 15;143(12):2160-71. doi: 10.1242/dev.132704. Epub 2016 Apr 27. PMID: 27122169; PMCID: PMC4920172.

[9]. Schneider L, Clement CA, Teilmann SC, Pazour GJ, Hoffmann EK, Satir P, Christensen ST. PDGFRalphaalpha signaling is regulated through the primary cilium in fibroblasts. Curr Biol. 2005 Oct 25;15(20):1861-6. doi: 10.1016/j.cub.2005.09.012. PMID: 16243034.

[10]. Christensen ST, Clement CA, Satir P, Pedersen LB. Primary cilia and coordination of receptor tyrosine kinase (RTK) signalling. J Pathol. 2012 Jan;226(2):172-84. doi: 10.1002/path.3004. Epub 2011 Nov 21. PMID:

21956154; PMCID: PMC4294548.

[11]. Rimkus TK, Carpenter RL, Qasem S, Chan M, Lo HW. Targeting the Sonic Hedgehog Signaling Pathway: Review of Smoothened and GLI Inhibitors. Cancers (Basel). 2016 Feb 15;8(2):22. doi: 10.3390/cancers8020022. PMID: 26891329; PMCID: PMC4773745.

[12]. Dilower I, Niloy AJ, Kumar V, Kothari A, Lee EB, Rumi MAK. Hedgehog Signaling in Gonadal Development and Function. Cells. 2023 Jan 18;12(3):358. doi: 10.3390/cells12030358. PMID: 36766700; PMCID: PMC9913308.

[13]. Lepage T, Cohen SM, Diaz-Benjumea FJ, Parkhurst SM. Signal transduction by cAMP-dependent protein kinase A in Drosophila limb patterning. Nature. 1995 Feb 23;373(6516):711-5. doi: 10.1038/373711a0. PMID: 7854456.

[14]. Li W, Ohlmeyer JT, Lane ME, Kalderon D. Function of protein kinase A in hedgehog signal transduction and Drosophila imaginal disc development. Cell. 1995 Feb 24;80(4):553-62. doi: 10.1016/0092-8674(95)90509-x. PMID: 7867063.

[15]. Hammerschmidt M, Bitgood MJ, McMahon AP. Protein kinase A is a common negative regulator of Hedgehog signaling in the vertebrate embryo. Genes Dev. 1996 Mar 15;10(6):647-58. doi: 10.1101/gad.10.6.647. PMID: 8598293.

[16]. Robbins DJ, Nybakken KE, Kobayashi R, Sisson JC, Bishop JM, Thérond PP. Hedgehog elicits signal transduction by means of a large complex containing the kinesin-related protein costal2. Cell. 1997 Jul 25;90(2):225-34. doi: 10.1016/s0092-8674(00)80331-1. PMID: 9244297.

[17]. Zhang P, Knape MJ, Ahuja LG, Keshwani MM, King CC, Sastri M, Herberg FW, Taylor SS. Single Turnover Autophosphorylation Cycle of the PKA RII β Holoenzyme. PLoS Biol. 2015 Jul 9;13(7):e1002192. doi: 10.1371/journal.pbio.1002192. PMID: 26158466; PMCID: PMC4497662.

[18]. Rosenberg D, Groussin L, Jullian E, Perlemoine K, Bertagna X, Bertherat J. Role of the PKA-regulated transcription factor CREB in development and tumorigenesis of endocrine tissues. Ann N Y Acad Sci. 2002 Jun;968:65-74. doi: 10.1111/j.1749-6632.2002.tb04327.x. PMID: 12119268.

[19]. Bollen E, Puzzo D, Rutten K, Privitera L, De Vry J, Vanmierlo T, Kenis G, Palmeri A, D'Hooge R, Balschun D, Steinbusch HM, Blokland A, Prickaerts J. Improved long-term memory via enhancing cGMP-PKG signaling requires cAMP-PKA signaling. Neuropsychopharmacology. 2014 Oct;39(11):2497-505. doi: 10.1038/npp.2014.106. Epub 2014 May 12. PMID: 24813825; PMCID: PMC4207334.

[20]. Torella D, Gasparri C, Ellison GM, Curcio A, Leone A, Vicinanza C, Galuppo V, Mendicino I, Sacco W, Aquila I, Surace FC, Luposella M, Stillo G, Agosti V, Cosentino C, Avvedimento EV, Indolfi C. Differential regulation of vascular smooth muscle and endothelial cell proliferation in vitro and in vivo by cAMP/PKA-activated p85alphaPI3K. Am J Physiol Heart Circ Physiol. 2009 Dec;297(6):H2015-25. doi: 10.1152/ajpheart.00738.2009. Epub 2009 Sep 25. PMID: 19783773.

[21]. Torres-Quesada O, Mayrhofer JE, Stefan E. The many faces of compartmentalized PKA signalosomes. Cell Signal. 2017 Sep;37:1-11. doi: 10.1016/j.cellsig.2017.05.012. Epub 2017 May 18. PMID: 28528970.

[22]. DeCamp DL, Thompson TM, de Sauvage FJ, Lerner MR. Smoothened activates Galphai-mediated signaling in frog melanophores. J Biol Chem. 2000 Aug 25;275(34):26322-7. doi: 10.1074/jbc.M004055200. PMID: 10835429.

[23]. Shen F, Cheng L, Douglas AE, Riobo NA, Manning DR. Smoothened is a fully competent activator of the heterotrimeric G protein G(i). Mol Pharmacol. 2013 Mar;83(3):691-7. doi: 10.1124/mol.112.082511. Epub 2013 Jan 4. PMID: 23292797; PMCID: PMC3583497.

[24]. Mukhopadhyay S, Wen X, Ratti N, Loktev A, Rangell L, Scales SJ, Jackson PK. The ciliary G-protein-coupled receptor Gpr161 negatively regulates the Sonic hedgehog pathway via cAMP signaling. Cell. 2013 Jan 17;152(1-2):210-23. doi: 10.1016/j.cell.2012.12.026. PMID: 23332756.

[25]. Ni Q, Titov DV, Zhang J. Analyzing protein kinase dynamics in living cells with FRET reporters. Methods. 2006 Nov;40(3):279-86. doi: 10.1016/j.ymeth.2006.06.013. PMID: 16908183.

[26]. MD, Zhang J. Subcellular dynamics of protein kinase A activity visualized by FRET-based reporters. Biochem Biophys Res Commun. 2006 Sep 22;348(2):716-21. doi: 10.1016/j.bbrc.2006.07.136. Epub 2006 Jul 31. PMID: 16895723.

[27]. hijima S, Okamoto H, Ueno N, Hotta Y, Eguchi G. High-frequency generation of transgenic zebrafish which reliably express GFP in whole muscles or the whole body by using promoters of zebrafish origin. Dev Biol. 1997 Dec 15;192(2):289-99. doi: 10.1006/dbio.1997.8779. PMID: 9441668.

[28]. Concordet JP, Lewis KE, Moore JW, Goodrich LV, Johnson RL, Scott MP, Ingham PW. Spatial regulation of a zebrafish patched homologue reflects the roles of sonic hedgehog and protein kinase A in neural tube and somite patterning. Development. 1996 Sep;122(9):2835-46. doi: 10.1242/dev.122.9.2835. PMID: 8787757.

[29]. Johnson RL, Grenier JK, Scott MP. patched overexpression alters wing disc size and pattern: transcriptional and post-transcriptional effects on hedgehog targets. Development. 1995 Dec;121(12):4161-70. doi: 10.1242/dev.121.12.4161. PMID: 8575316.

[30]. Hammerschmidt M, Bitgood MJ, McMahon AP. Protein kinase A is a common negative regulator of Hedgehog signaling in the vertebrate embryo. Genes Dev. 1996 Mar 15;10(6):647-58. doi: 10.1101/gad.10.6.647. PMID: 8598293.

[31]. Zhang H, Huang Z, Lv L, Xin Y, Wang Q, Li F, Dong L, Wu C, Ingham

PW, Zhao Z. A transgenic zebrafish for in vivo visualization of cilia. Open Biol. 2022 Aug;12(8):220104. doi: 10.1098/rsob.220104. Epub 2022 Aug 10. PMID: 35946311; PMCID: PMC9364149.

[32]. Truong ME, Bilekova S, Choksi SP, Li W, Bugaj LJ, Xu K, Reiter JF. Vertebrate cells differentially interpret ciliary and extraciliary cAMP. Cell. 2021 May 27;184(11):2911-2926.e18. doi: 10.1016/j.cell.2021.04.002. Epub 2021 Apr 30. PMID: 33932338; PMCID: PMC8450001.

[33]. Scott JD, Pawson T. Cell signaling in space and time: where proteins come together and when they're apart. Science. 2009 Nov 27;326(5957):1220-4. doi: 10.1126/science.1175668. PMID: 19965465; PMCID: PMC3041271.

[34]. Taylor SS, Yang J, Wu J, Haste NM, Radzio-Andzelm E, Anand G. PKA: a portrait of protein kinase dynamics. Biochim Biophys Acta. 2004 Mar 11;1697(1-2):259-69. doi: 10.1016/j.bbapap.2003.11.029. PMID: 15023366.

[35]. Mick DU, Rodrigues RB, Leib RD, Adams CM, Chien AS, Gygi SP, Nachury MV. Proteomics of Primary Cilia by Proximity Labeling. Dev Cell. 2015 Nov 23;35(4):497-512. doi: 10.1016/j.devcel.2015.10.015. Epub 2015 Nov 12. PMID: 26585297; PMCID: PMC4662609.

[36]. Wolff C, Roy S, Ingham PW. Multiple muscle cell identities induced by distinct levels and timing of hedgehog activity in the zebrafish embryo. Curr Biol. 2003 Jul 15;13(14):1169-81. doi: 10.1016/s0960-9822(03)00461-5. PMID: 12867027.

[37]. Maurya AK, Ben J, Zhao Z, Lee RT, Niah W, Ng AS, Iyu A, Yu W, Elworthy S, van Eeden FJ, Ingham PW. Positive and negative regulation of Gli activity by Kif7 in the zebrafish embryo. PLoS Genet. 2013;9(12):e1003955. doi: 10.1371/journal.pgen.1003955. Epub 2013 Dec 5. PMID: 24339784; PMCID: PMC3854788.

[38]. Wolff C, Roy S, Lewis KE, Schauerte H, Joerg-Rauch G, Kirn A, Weiler C, Geisler R, Haffter P, Ingham PW. iguana encodes a novel zinc-finger

protein with coiled-coil domains essential for Hedgehog signal transduction in the zebrafish embryo. Genes Dev. 2004 Jul 1;18(13):1565-76. doi: 10.1101/gad.296004. Epub 2004 Jun 15. PMID: 15198976; PMCID: PMC443519.

[39]. Tay SY, Yu X, Wong KN, Panse P, Ng CP, Roy S. The iguana/DZIP1 protein is a novel component of the ciliogenic pathway essential for axonemal biogenesis. Dev Dyn. 2010 Feb;239(2):527-34. doi: 10.1002/dvdy.22199. PMID: 20014402.

[40]. Chen H, Wu Z, Yan Z, Chen C, Zhang Y, Wang Q, Gao Y, Ling K, Hu J, Wei Q. The ARPKD Protein DZIP1L Regulates Ciliary Protein Entry by Modulating the Architecture and Function of Ciliary Transition Fibers. Adv Sci (Weinh). 2024 Jun;11(24):e2308820. doi: 10.1002/advs.202308820. Epub 2024 Apr 17. PMID: 38634253; PMCID: PMC11200010.

[41]. Tempé D, Casas M, Karaz S, Blanchet-Tournier MF, Concordet JP. Multisite protein kinase A and glycogen synthase kinase 3beta phosphorylation leads to Gli3 ubiquitination by SCFbetaTrCP. Mol Cell Biol. 2006 Jun;26(11):4316-26. doi: 10.1128/MCB.02183-05. PMID: 16705181; PMCID: PMC1489100.

[42]. Pan Y, Wang C, Wang B. Phosphorylation of Gli2 by protein kinase A is required for Gli2 processing and degradation and the Sonic Hedgehog-regulated mouse development. Dev Biol. 2009 Feb 1;326(1):177-89. doi: 10.1016/j.ydbio.2008.11.009. Epub 2008 Nov 20. PMID: 19056373; PMCID: PMC2650378.

[43]. Niewiadomski P, Kong JH, Ahrends R, Ma Y, Humke EW, Khan S, Teruel MN, Novitch BG, Rohatgi R. Gli protein activity is controlled by multisite phosphorylation in vertebrate Hedgehog signaling. Cell Rep. 2014 Jan 16;6(1):168-181. doi: 10.1016/j.celrep.2013.12.003. Epub 2013 Dec 27. PMID: 24373970; PMCID: PMC3915062.

[44]. Walker MF, Zhang J, Steiner W, Ku PI, Zhu JF, Michaelson Z, Yen YC,

Lee A, Long AB, Casey MJ, Poddar A, Nelson IB, Arveseth CD, Nagel F, Clough R, LaPotin S, Kwan KM, Schulz S, Stewart RA, Tesmer JJG, Caspary T, Subramanian R, Ge X, Myers BR. GRK2 kinases in the primary cilium initiate SMOOTHENED-PKA signaling in the Hedgehog cascade. PLoS Biol. 2024 Aug 13;22(8):e3002685. doi: 10.1371/journal.pbio.3002685. PMID: 39138140; PMCID: PMC11322411.

[45]. Li X, Wang X, Snyder M. Systematic investigation of protein-small molecule interactions. IUBMB Life. 2013 Jan;65(1):2-8. doi: 10.1002/iub.1111. Epub 2012 Dec 7. PMID: 23225626.

[46]. Wong W, Scott JD. AKAP signalling complexes: focal points in space and time. Nat Rev Mol Cell Biol. 2004 Dec;5(12):959-70. doi: 10.1038/nrm1527. PMID: 15573134.

[47]. Taylor SS, Ilouz R, Zhang P, Kornev AP. Assembly of allosteric macromolecular switches: lessons from PKA. Nat Rev Mol Cell Biol. 2012 Oct;13(10):646-58. doi: 10.1038/nrm3432. Epub 2012 Sep 20. PMID: 22992589; PMCID: PMC3985763.

[48]. Tewson PH, Martinka S, Shaner NC, Hughes TE, Quinn AM. New DAG and cAMP Sensors Optimized for Live-Cell Assays in Automated Laboratories. J Biomol Screen. 2016 Mar;21(3):298-305. doi: 10.1177/1087057115618608. Epub 2015 Dec 11. PMID: 26657040; PMCID: PMC4766961.

[49]. Moore BS, Stepanchick AN, Tewson PH, Hartle CM, Zhang J, Quinn AM, Hughes TE, Mirshahi T. Cilia have high cAMP levels that are inhibited by Sonic Hedgehog-regulated calcium dynamics. Proc Natl Acad Sci U S A. 2016 Nov 15;113(46):13069-13074. doi: 10.1073/pnas.1602393113. Epub 2016 Oct 31. PMID: 27799542; PMCID: PMC5135322.

[50]. Jiang JY, Falcone JL, Curci S, Hofer AM. Direct visualization of cAMP signaling in primary cilia reveals up-regulation of ciliary GPCR activity following Hedgehog activation. Proc Natl Acad Sci U S A. 2019 Jun

11;116(24):12066-12071. doi: 10.1073/pnas.1819730116. Epub 2019 May 29. PMID: 31142652; PMCID: PMC6575585.

[51]. Beavo JA, Brunton LL. Cyclic nucleotide research -- still expanding after half a century. Nat Rev Mol Cell Biol. 2002 Sep;3(9):710-8. doi: 10.1038/nrm911. PMID: 12209131.

[52]. Tuson M, He M, Anderson KV. Protein kinase A acts at the basal body of the primary cilium to prevent Gli2 activation and ventralization of the mouse neural tube. Development. 2011 Nov;138(22):4921-30. doi: 10.1242/dev.070805. Epub 2011 Oct 17. PMID: 22007132; PMCID: PMC3201661.

[53]. Peng H, Zhang J, Ya A, Ma W, Villa S, Sukenik S, Ge X. Myomegalin regulates Hedgehog pathway by controlling PDE4D at the centrosome. Mol Biol Cell. 2021 Sep 1;32(19):1807-1817. doi: 10.1091/mbc.E21-02-0064. Epub 2021 Jul 14. PMID: 34260267; PMCID: PMC8684712.

[54]. Paolocci E, Zaccolo M. Compartmentalised cAMP signalling in the primary cilium. Front Physiol. 2023 May 9;14:1187134. doi: 10.3389/fphys.2023.1187134. PMID: 37256063; PMCID: PMC10226274.

[55]. Berman DM, Karhadkar SS, Hallahan AR, Pritchard JI, Eberhart CG, Watkins DN, Chen JK, Cooper MK, Taipale J, Olson JM, Beachy PA. Medulloblastoma growth inhibition by hedgehog pathway blockade. Science. 2002 Aug 30;297(5586):1559-61. doi: 10.1126/science.1073733. PMID: 12202832.

[56]. Epstein EH. Basal cell carcinomas: attack of the hedgehog. Nat Rev Cancer. 2008 Oct;8(10):743-54. doi: 10.1038/nrc2503. PMID: 18813320; PMCID: PMC4457317.

[57]. Skoda AM, Simovic D, Karin V, Kardum V, Vranic S, Serman L. The role of the Hedgehog signaling pathway in cancer: A comprehensive review. Bosn J Basic Med Sci. 2018 Feb 20;18(1):8-20. doi: 10.17305/bjbms.2018.2756. PMID: 29274272; PMCID: PMC5826678.

[58]. Walton KD, Gumucio DL. Hedgehog Signaling in Intestinal Development and Homeostasis. Annu Rev Physiol. 2021 Feb 10;83:359-380. doi: 10.1146/annurev-physiol-031620-094324. Epub 2020 Oct 9. PMID: 33035430; PMCID: PMC10278198.

[59]. Kimmel CB, Ballard WW, Kimmel SR, Ullmann B, Schilling TF. Stages of embryonic development of the zebrafish. Dev Dyn. 1995 Jul;203(3):253-310. doi: 10.1002/aja.1002030302. PMID: 8589427.

[60]. Montague TG, Cruz JM, Gagnon JA, Church GM, Valen E. CHOPCHOP: a CRISPR/Cas9 and TALEN web tool for genome editing. Nucleic Acids Res. 2014 Jul;42(Web Server issue):W401-7. doi: 10.1093/nar/gku410. Epub 2014 May 26. PMID: 24861617; PMCID: PMC4086086.

[61]. Wang M, Li P, Wang H, Dong L, Wu C, Zhao Z. Identification and spatiotemporal expression of gpr161 genes in zebrafish. Gene. 2020 Mar 10;730:144303. doi: 10.1016/j.gene.2019.144303. Epub 2019 Dec 26. PMID: 31884103.

[62]. Karpova TS, Baumann CT, He L, Wu X, Grammer A, Lipsky P, Hager GL, McNally JG. Fluorescence resonance energy transfer from cyan to yellow fluorescent protein detected by acceptor photobleaching using confocal microscopy and a single laser. J Microsc. 2003 Jan;209(Pt 1):56-70. doi: 10.1046/j.1365-2818.2003.01100.x. PMID: 12535185.

[63]. Thisse C, Thisse B. High-resolution in situ hybridization to whole-mount zebrafish embryos. Nat Protoc. 2008;3(1):59-69. doi: 10.1038/nprot.2007.514. PMID: 18193022.

[64]. Endoh-Yamagami S, Evangelista M, Wilson D, Wen X, Theunissen JW, Phamluong K, Davis M, Scales SJ, Solloway MJ, de Sauvage FJ, Peterson AS. The mammalian Cos2 homolog Kif7 plays an essential role in modulating HH signal transduction during development. Curr Biol. 2009 Aug 11;19(15):1320-6. doi: 10.1016/j.cub.2009.06.046. Epub 2009 Jul 9. PMID: 19592253.

[65]. Huangfu D, Liu A, Rakeman AS, Murcia NS, Niswander L, Anderson KV. Hedgehog signalling in the mouse requires intraflagellar transport proteins. Nature. 2003 Nov 6;426(6962):83-7. doi: 10.1038/nature02061. PMID: 14603322.

[66]. Bazzi H, Anderson KV. Acentriolar mitosis activates a p53-dependent apoptosis pathway in the mouse embryo. Proc Natl Acad Sci U S A. 2014 Apr 15;111(15):E1491-500. doi: 10.1073/pnas.1400568111. Epub 2014 Mar 31. PMID: 24706806; PMCID: PMC3992648.

[67]. Davey MG, Paton IR, Yin Y, Schmidt M, Bangs FK, Morrice DR, Smith TG, Buxton P, Stamataki D, Tanaka M, Münsterberg AE, Briscoe J, Tickle C, Burt DW. The chicken talpid3 gene encodes a novel protein essential for Hedgehog signaling. Genes Dev. 2006 May 15;20(10):1365-77. doi: 10.1101/gad.369106. PMID: 16702409; PMCID: PMC1472910.

[68]. Ogden SK, Fei DL, Schilling NS, Ahmed YF, Hwa J, Robbins DJ. G protein Galphai functions immediately downstream of Smoothened in Hedgehog signalling. Nature. 2008 Dec 18;456(7224):967-70. doi: 10.1038/nature07459. PMID: 18987629; PMCID: PMC2744466.

[69]. May EA, Kalocsay M, D'Auriac IG, Schuster PS, Gygi SP, Nachury MV, Mick DU. Time-resolved proteomics profiling of the ciliary Hedgehog response. J Cell Biol. 2021 May 3;220(5):e202007207. doi: 10.1083/jcb.202007207. PMID: 33856408; PMCID: PMC8054476

[70]. Ben J, Elworthy S, Ng AS, van Eeden F, Ingham PW. Targeted mutation of the talpid3 gene in zebrafish reveals its conserved requirement for ciliogenesis and Hedgehog signalling across the vertebrates. Development. 2011 Nov;138(22):4969-78. doi: 10.1242/dev.070862. PMID: 22028029; PMCID: PMC3201664.

[71]. Tsurumi Y, Hamada Y, Katoh Y, Nakayama K. Interactions of the dynein-2 intermediate chain WDR34 with the light chains are required for ciliary retrograde protein trafficking. Mol Biol Cell. 2019 Mar 1;30(5):658-670.

doi: 10.1091/mbc.E18-10-0678. Epub 2019 Jan 16. PMID: 30649997; PMCID: PMC6589695.

[72]. Expression of zebrafish nk2.2 is influenced by sonic hedgehog/vertebrate hedgehog-1 and demarcates a zone of neuronal differentiation in the embryonic forebrain.

[73]. Stamataki D, Ulloa F, Tsoni SV, Mynett A, Briscoe J. A gradient of Gli activity mediates graded Sonic Hedgehog signaling in the neural tube. Genes Dev. 2005 Mar 1;19(5):626-41. doi: 10.1101/gad.325905. PMID: 15741323; PMCID: PMC551582.

FIGURE LEGENDS

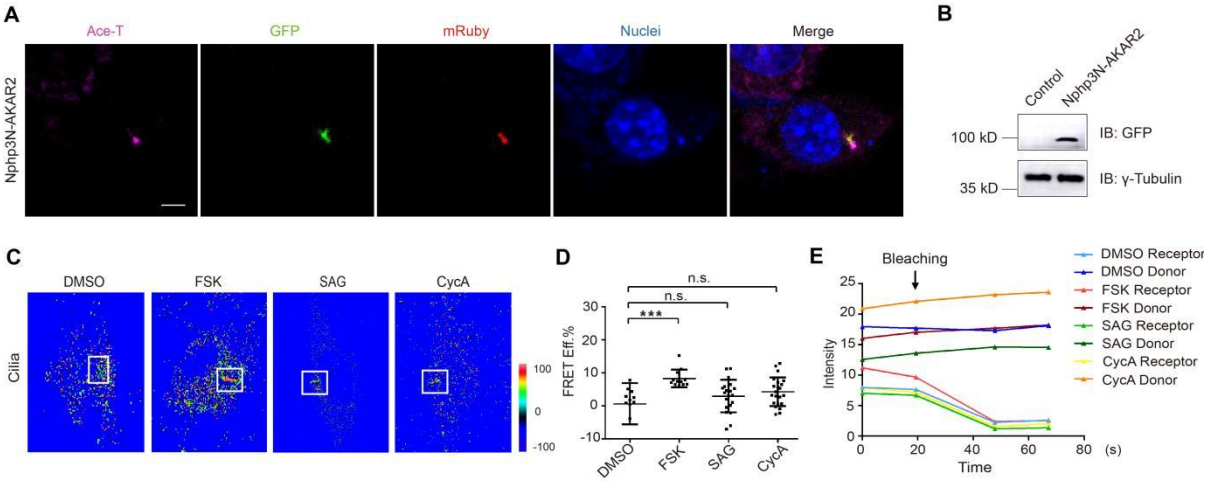

Figure 1. The Nphp3N-AKAR2-CR can efficiently sense the ciliary PKA activity in NIH3T3 cells. (A) Specifically ciliary localization of Nphp3N-AKAR2-CR as indicated by colocalization of Clover in green, mRuby in red with cilium stained by acetated tubulin in purple. The nuclei were labelled in blue by Hoechst. Scale bars, 5 μm. (B) The expression of Nphp3N-AKAR2-CR was detected by immunoblot using GFP antibody against AKAR2-CR. The γ-tubulin was used as loading control. (C) The FRET ratio image of ciliary AKAR2-CR in NIH3T3 cells treated with DMSO, 10 μM Foskolin (FSK), 1 μM SAG and 5 μM cyclopamine (CYC), respectively. (D) Statistical analysis of the ciliary FRET efficiency in NIH3T3 cells in response to DMSO, FSK, SAG and CYC, respectively (n_{DMSO}=12 cilia, n_{FSK}=12 cilia, n_{SAG}=20 cilia n_{CYC}=22 cilia). Unpaired Student's *t*-test was performed, and the ns indicates 'not significant' with P>0.05, while *** indicates 'significant' with $P<0.0001$. (E) Mean ciliary fluorescence intensity changes of both acceptors and donors of Nphp3N-AKAR2-CR in FRET assay on NIH3T3 cells treated with DMSO, FSK, SAG, and CYC.

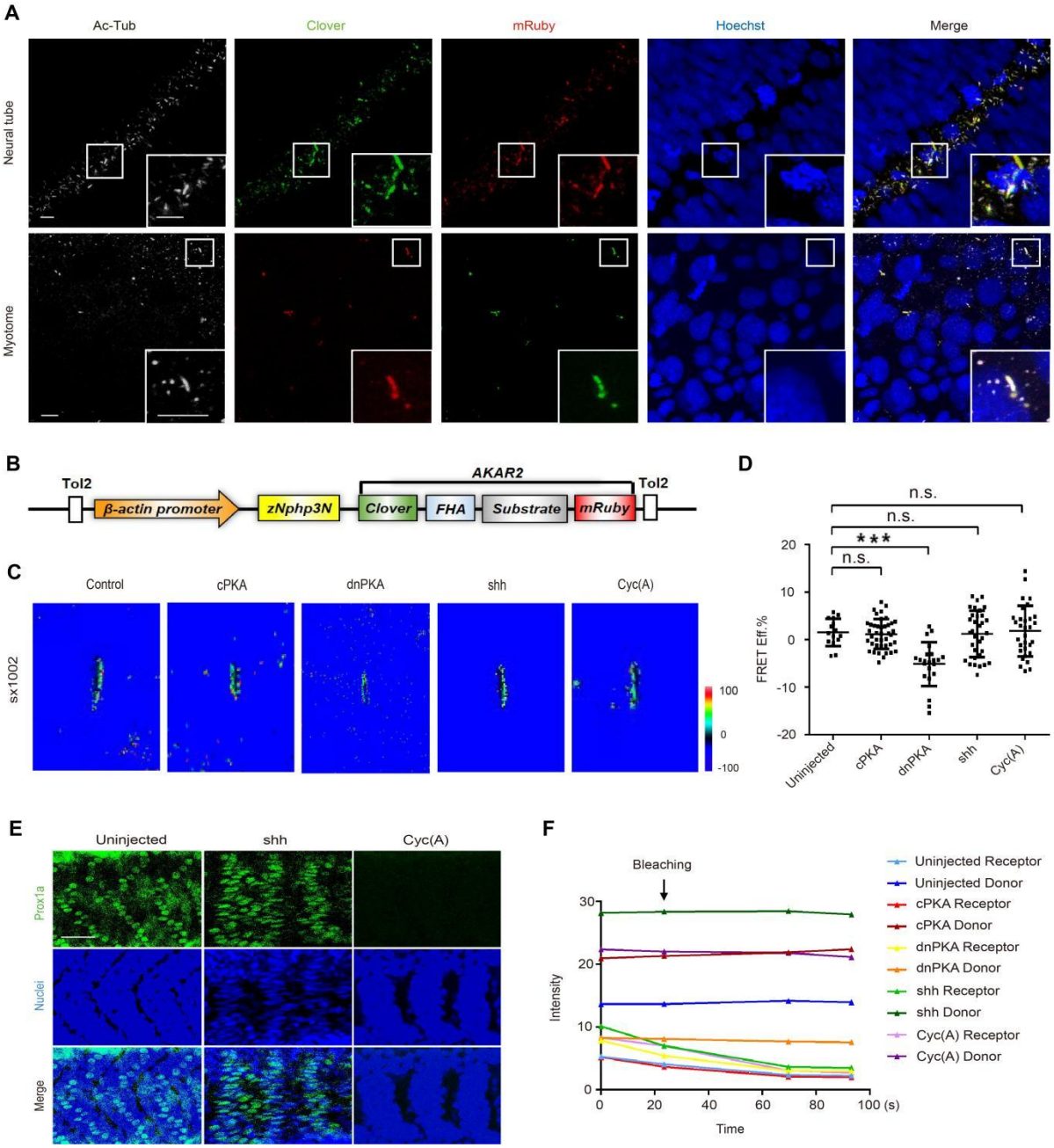

Figure 2. PKA activity can effectively detected in PC of *sx1002* embryos. (A) The transiently expressed zNphp3N-AKAR2 in zebrafish embryos as indicated by Clover in green and mRuby in red was efficiently localized in the primary cilia of cells in the neural tube and myotome. Cilia were labeled by AcTub in gray. Each small frame on the lower right corner of the main frame denotes the enlarged site as encircled by white square. The nuclei were labelled by Hoechst in blue. Scale bar, 5 μm. (B) Schematic diagram of the *Nphp3N-AKAR2-CR* vector used for generating the transgenic ciliary PKA reporter zebrafish. (C) The FRET

ratio image of ciliary AKAR2-CR in *sx1002* injected with cPKA, dnPKA, and *shh* mRNA, respectively, or treated with CycA. (D) Statistical analysis of the ciliary FRET efficiency in *sx1002* treated with cPKA, dnPKA, *shh* and Cyc(A) ($n_{uninjected}$=18 cilia, n_{cPKA}=40 cilia, n_{dnPKA}=24 cilia, n_{shh}=33 cilia n_{cycA}=31 cilia). Unpaired Student's *t*-test was performed, and the ns indicates 'not significant' with P>0.05, while *** indicates 'significant' with *P*<0.0001 (E) Representative Prox1a (red)/nuclei (blue) immunostainings of *sx1002* embryos at 24 hpf after injected with *shh* mRNA or treated with Cyc(A), respectively. (F) Mean ciliary fluorescence intensity changes of both acceptors and donors of Nphp3N-AKAR2-CR in FRET assay on *sx1002* injected with cPKA, dnPKA, and *shh* mRNA, respectively, or treated with CycA.

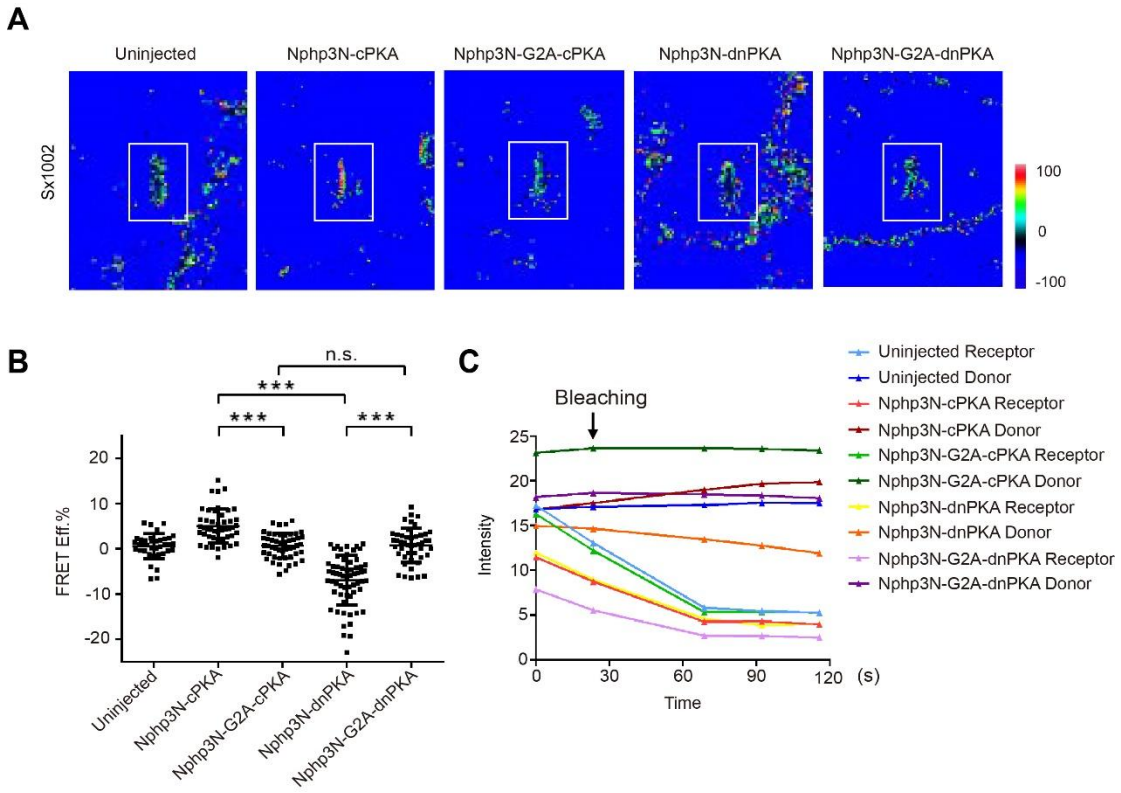

Figure 3. Ciliary cPKA and dnPKA modulated the ciliary PKA activity. (A) The FRET ratio image of ciliary AKAR2-CR in *sx1002* expressing either the Cilia-cPKA/dnPKA or Cyto-cPKA/dnPKA. Representative images of the FRET ratio for each condition in the pseudocolor scale. (B) Statistical analysis of the ciliary FRET efficiency in *sx1002* expressing

either Cilia-cPKA/dnPKA or Cyto-cPKA/dnPKA ($n_{uninjected}$=37 cilia, $n_{Nphp3N\text{-}cPKA}$=46 cilia, $n_{Nphp3N\text{-}G2A\text{-}cPKA}$=49 cilia, $n_{Nphp3N\text{-}dnPKA}$=54 cilia, $n_{Nphp3N\text{-}G2A\text{-}cPKA}$=46 cilia). Unpaired Student's *t*-test was performed, and the ns indicates 'not significance' with P>0.05, while *** indicates 'significant' with *P*<0.0001 (C) Mean ciliary fluorescence intensity changes of both acceptors and donors of Nphp3N-AKAR2-CR in FRET assay on *sx1002* expressing either Cilia-cPKA/dnPKA or Cyto-cPKA/dnPKA, respectively.

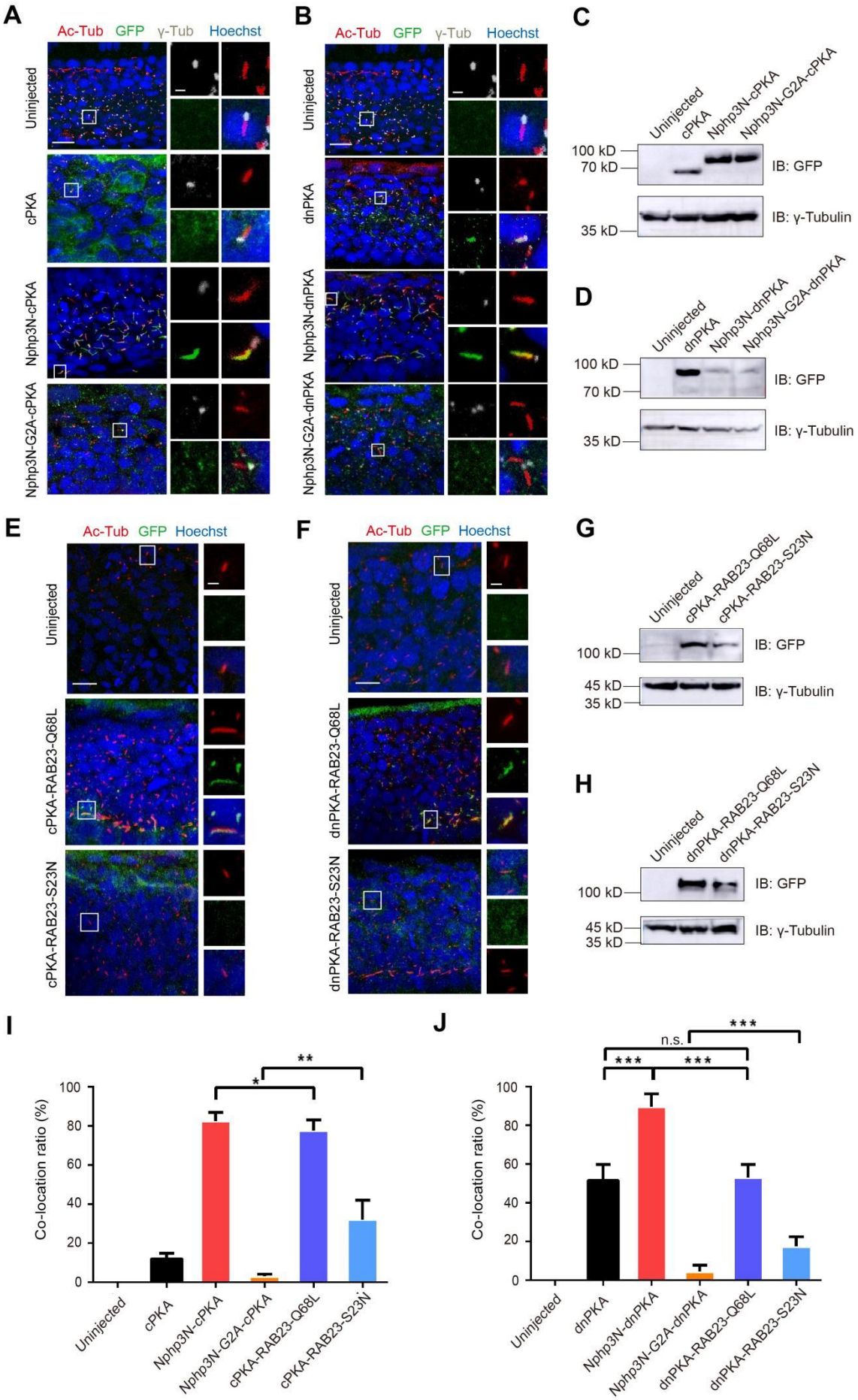
A
Ac-Tub GFP γ-Tub Hoechst
Uninjected
cPKA
Nphp3N-cPKA
Nphp3N-G2A-cPKA
B
Ac-Tub GFP γ-Tub Hoechst
Uninjected
dnPKA
Nphp3N-dnPKA
Nphp3N-G2A-dnPKA
C
Uninjected
cPKA
Nphp3N-cPKA
Nphp3N-G2A-cPKA
100 kD
70 kD
IB: GFP
35 kD
IB: γ-Tubulin
D
Uninjected
dnPKA
Nphp3N-dnPKA
Nphp3N-G2A-dnPKA
100 kD
70 kD
IB: GFP
35 kD
IB: γ-Tubulin
E
Ac-Tub GFP Hoechst
Uninjected
cPKA-RAB23-Q68L
cPKA-RAB23-S23N
F
Ac-Tub GFP Hoechst
Uninjected
dnPKA-RAB23-Q68L
dnPKA-RAB23-S23N
G
Uninjected
cPKA-RAB23-Q68L
cPKA-RAB23-S23N
100 kD
IB: GFP
45 kD
35 kD
IB: γ-Tubulin
H
Uninjected
dnPKA-RAB23-Q68L
dnPKA-RAB23-S23N
100 kD
IB: GFP
45 kD
35 kD
IB: γ-Tubulin
I
Co-location ratio (%)
100
80
60
40
20
0
*
**
Uninjected
cPKA
Nphp3N-cPKA
Nphp3N-G2A-cPKA
cPKA-RAB23-Q68L
cPKA-RAB23-S23N
J
Co-location ratio (%)
100
80
60
40
20
0
n.s.
***
***
***
Uninjected
dnPKA
Nphp3N-dnPKA
Nphp3N-G2A-dnPKA
dnPKA-RAB23-Q68L
dnPKA-RAB23-S23N

Figure 4. Nphp3N drove cilia localization of the cPKA/dnPKA more efficiently than RAB23. (A and B) Subcellular localization of the cPKA/dnPKA-eGFP, Nphp3N(WT/G2A)-cPKA/dnPKA-eGFP in embryos at 18 hpf, as indicated by eGFP in green. The cilia were labelled by Ac-Tub in red, the basal body by γ-tubulin in gray, and the nuclei by Hoechst in blue. Frames on the right panel indicates cilia depicted in the inset, with the basal body on upper left, cilia on upper right, indicated cPKAs/dnPKAs on lower left, and merge images on lower right. Scale bars, 10 μm for each left panel and 2.5 μm for the right panel. (C and D) Immunoblot of lysates from 18hpf zebrafish embryo expressing indicated GFP-tagged forms of Nphp3N-cPKAs/dnPKAs. The γ-tubulin was used as loading control. (E and F) Subcellular localization of the cPKA/dnPKA-eGFP-Rab23 Q68L/S23N in embryos at 18 hpf, as indicated by eGFP in green. The cilia were labelled by Ac-Tub in red, and the nuclei by Hoechst in blue. Frames on the right panel indicates cilia depicted in the inset, with cilia on the top, indicated cPKAs/dnPKAs in the middle, and merge images at the bottom. Scale bars, 10 μm for the left panel and 2.5 μm for the right panel. (G and H) Immunoblot of lysates from 18hpf zebrafish embryo expressing indicated GFP-tagged forms of RAB23-cPKAs/dnPKAs. The γ-tubulin was used as loading control. (I and J) Quantification of ciliary colocalization from experiments presented in C-H (n = 60 cilia in 3 embryos). Unpaired Student's t-test was used for analysis, and *** indicates 'significant' with $P<0.001$, ** indicates 'significant' with $P<0.05$, * indicates 'significant' with $P<0.01$, ns indicates 'not significant' with $P>0.05$.

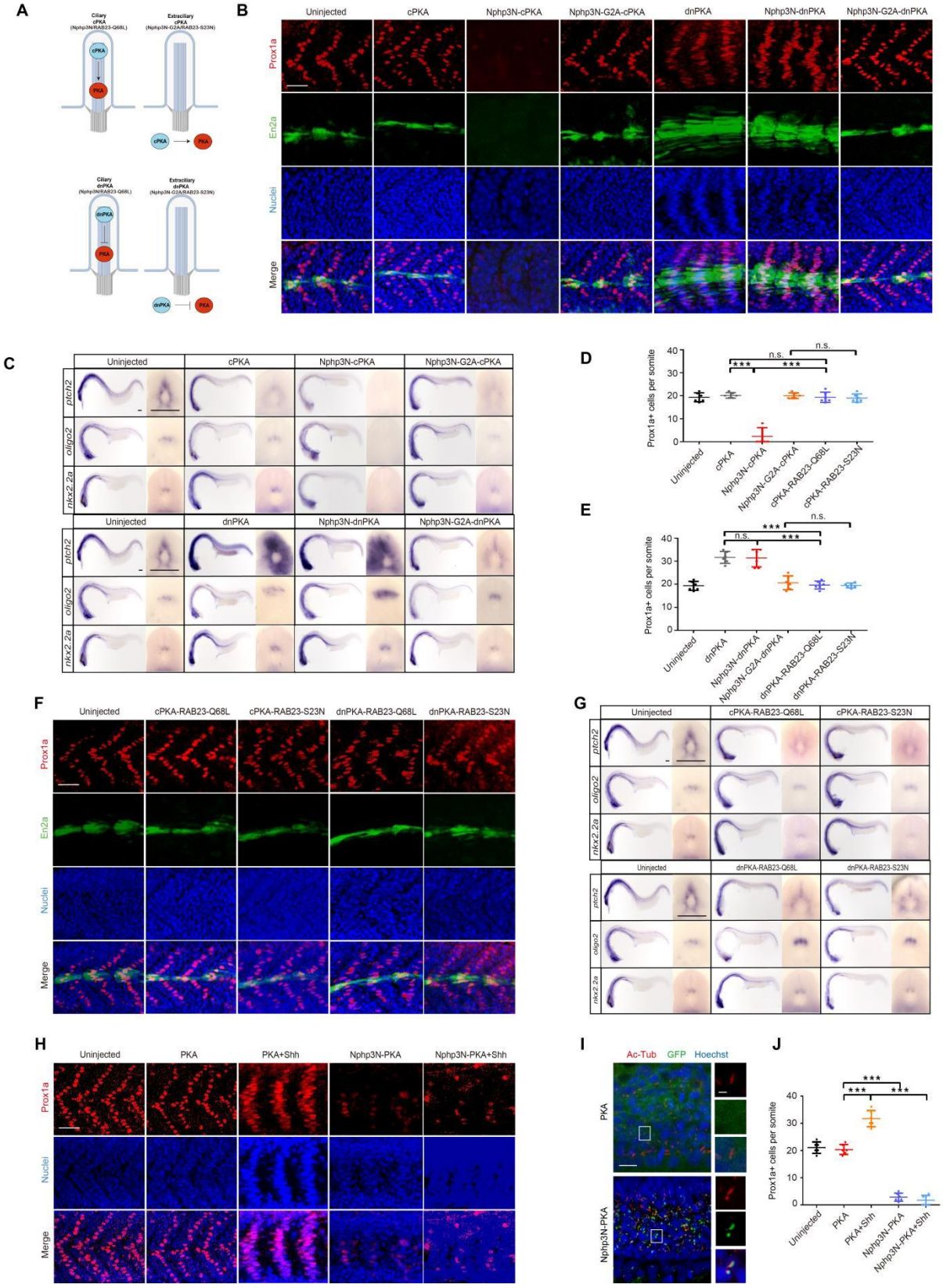

Figure 5. Ciliary but not cytosol PKA regulated HH signal transduction in zebrafish.

(A) Schematic digram of cPKA/dnPKA at distinct subcellular locations in this assay. The cPKA/dnPKA was delivered into the PC by Nphp3N as labeled by Cilia-cPKA/dnPKA, and

to the cytoplasm by Nphp3N-G2A as labeled by Cyto-cPKA/dnPKA. (B) The activity of Hh pathway was indicated by expression of Prox1a in red and En2a:eGFP in green in the embryos of Tg (*en2a*:*eGFP*)^{sx1005} expressing indicated Nphp3N (WT/G2A)-cPKA/dnPKA respectively. The nuclei were labelled by Hoechst in blue. Scale bar, 50 μm. (C and G) *In situ* hybridization of *ptch2*, *nkx2.2a* and *olig2* on the 24 hpf embryos expressing indicated cPKAs/dnPKAs. Each panel showed a full view of the embryo on the left and a cross-sectional view of a somite on the right (n = 3 for each sample). Scale bars, 100 μm. (D, E) Quantification of Prox1a+ cells from experiments presented in B and F (n = 6 somites from 3 embryos). Unpaired Student's t-test was performed. And ns indicates 'not significant' with P>0.05, *** indicates significant with P<0.001. (F) The activity of Hh pathway was indicated by expression of Prox1a in red and En2a:eGFP in green in the embryos of Tg (*en2a*:*eGFP*)^{sx1005} expressing RAB23 (Q68L/S23N)-cPKA/dnPKA respectively. The nuclei were labelled by Hoechst in blue. Scale bar, 50 μm. (H) The activity of Hh pathway was indicated by expression of Prox1a in red in the embryos of Tg (*en2a*:*eGFP*)^{sx1005} expressing PKA, PKA+SHH, Nphp3N-PKA or Nphp3N-PKA+SHH. The nuclei were labelled by Hoechst in blue. Scale bar, 50 μm. (I) Subcellular localization of the Nphp3N-PKA in embryos at 18 hpf, as indicated by eGFP in green. The cilia were labelled by Ac-Tub in red, and the nuclei by Hoechst in blue. Frames on the right panel indicates cilia depicted in the inset, with the cilia on the top, the indicated PKA in the middle, and merge layer at the bottom. Scale bars, 10 μm and 2.5 μm (inset). (J) Quantification of Prox1a+ cells from experiments presented in H (n = 6 somites in 3 embryos). Unpaired Student's t-test was used for analysis, ns indicates 'not significant' with P>0.05, *** indicates 'significant' with P<0.001.

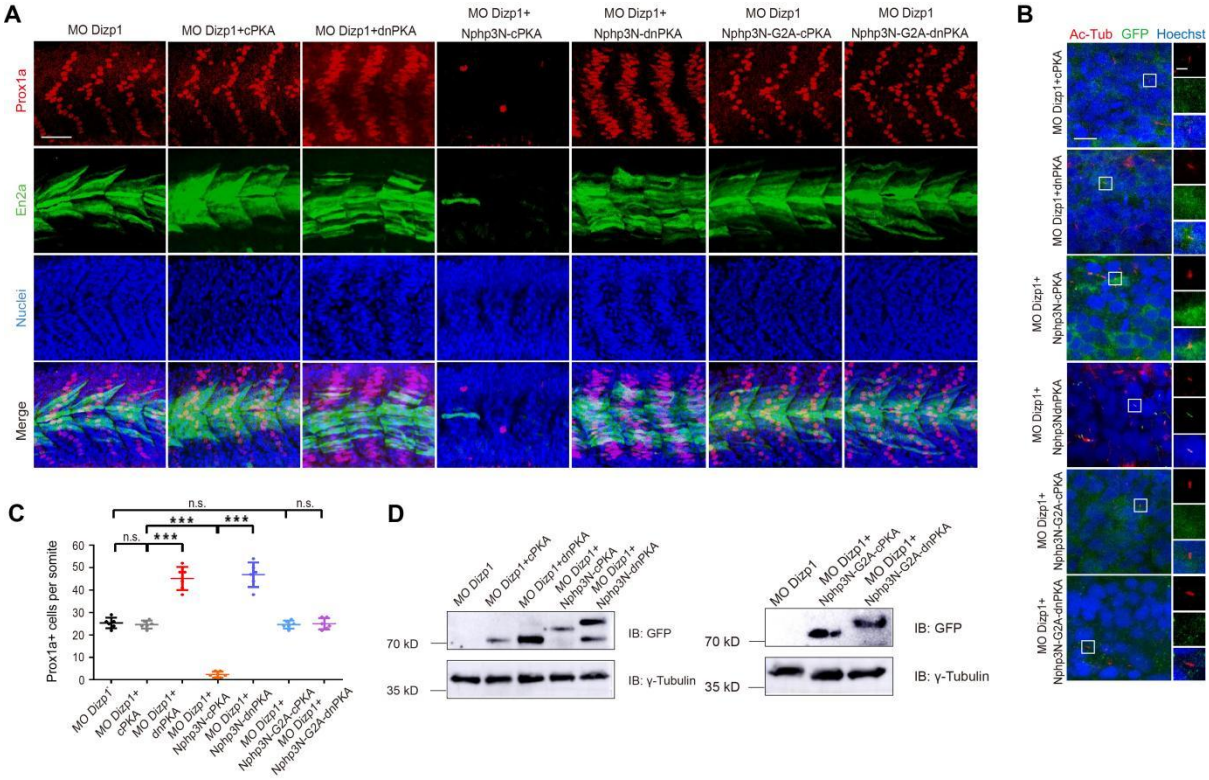

Figure 6. Cilia-cPKA/dnPKA specifically modulates Hh pathway even in absence of the PC in zebrafish embryos.

(A) The activity of Hh pathway was indicated by expression of Prox1a in red and En2a:eGFP in green in the embryos of Tg (*en2a*:*eGFP*)^{sx1005} injected with Dzip1 morpholino and indicated cPKA/dnPKA, respectively. The nuclei were labelled by Hoechst in blue. Scale bar, 50 μm. (B) Subcellular localization of the Nphp3N(WT/G2A)-cPKA/dnPKA in Dzip1 morphants at 18 hpf, as indicated by eGFP in green. The cilia were labelled by Ac-Tub in red, and the nuclei by Hoechst in blue. Frames on the right panel indicates cilia depicted in the inset, with the cilia on the top, the indicated PKA in the middle, and merge layer at the bottom. Scale bars, 10 μm and 2.5 μm (inset). (C) Quantification of Prox1a+ cells from experiments presented in A (n = 6 somites in 3 embryos). Unpaired Student's t-test was used for analysis. ns indicates 'not significant' with P>0.05. (D) Immunoblot of lysates from 18 hpf Dizp1 morphant embryos embryo expressing indicated GFP-tagged forms of cPKA/dnPKA. The γ-tubulin was used as loading control.

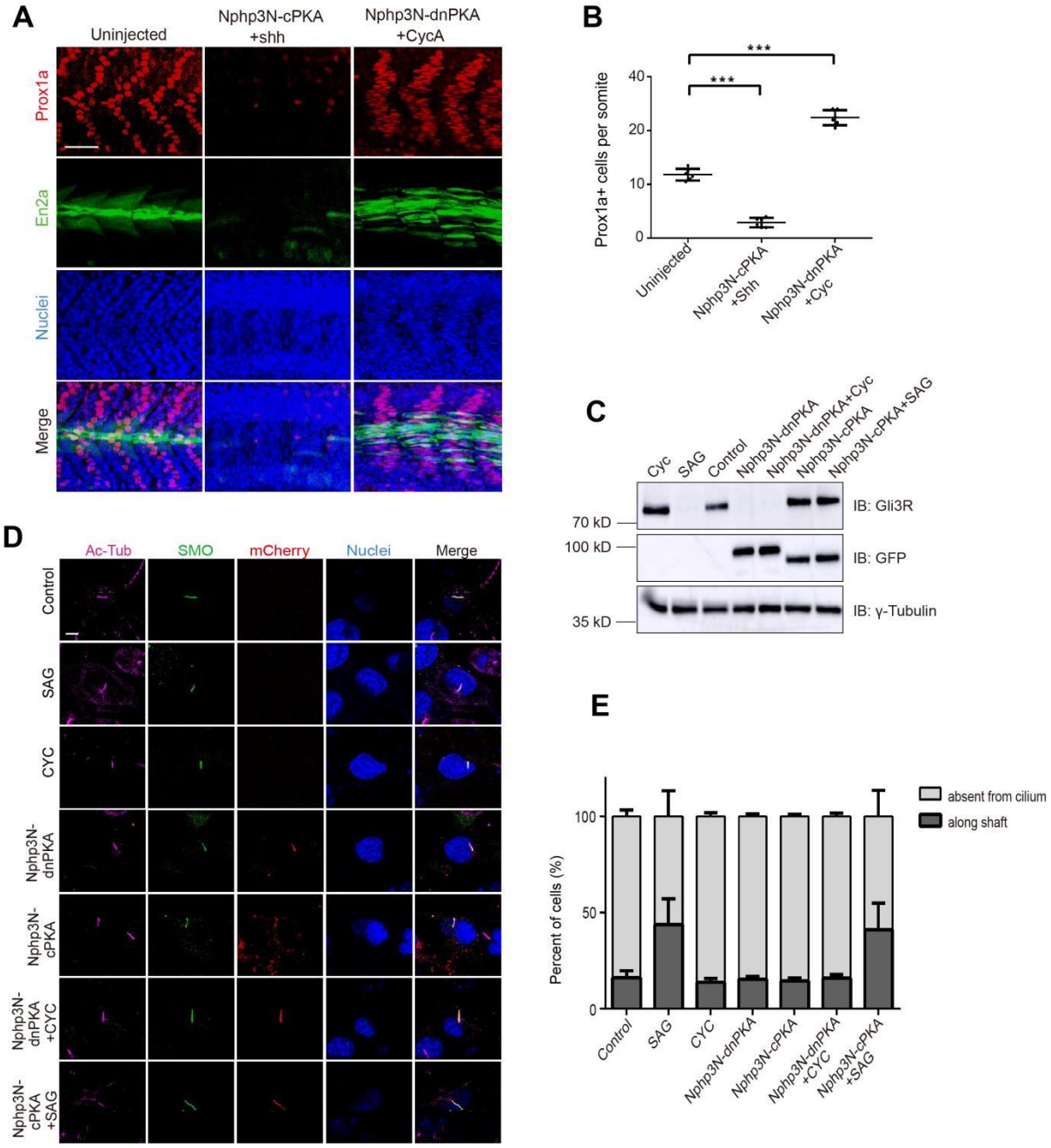

Figure 7. PKA was an essential and potent suppressor of the HH downstream pathway.

(A) The activity of Hh pathway was indicated by expression of Prox1a in red and En2a:eGFP in green in the embryos of Tg (*en2a*:*eGFP*)^{sx1005} with indicated treatment. The nuclei were labelled by Hoechst in blue. Scale bar, 50 μm. (B) Quantification of Prox1a+ cells from experiments presented in A (n = 6 somites in 3 embryos). Unpaired Student's t-test was performed. '***' indicates 'significant' with P<0.001. (C) Immunoblot of GLI3R in cell lines stably expressing Nphp3n-cPKA/dnPKA-GFP after treating with SAG or Cyc(A),

respectively. The γ-tubulin was used as loading control. (D) Subcellular localization of SMO in the NIH3T3 cells with indicated treatment as indicated in green. The ciliary expression of Nphp3N-cPKA/dnPKA were indicated by mCherry in red, the cilia were labeled by Ac-Tub in purple, and nuclei by Hoechst in blue. Scale bar, 5 μm. (B) Quantification of the proportion of cells with ciliary SMO from experiments presented in A. (n≥50 cilia for each assay).

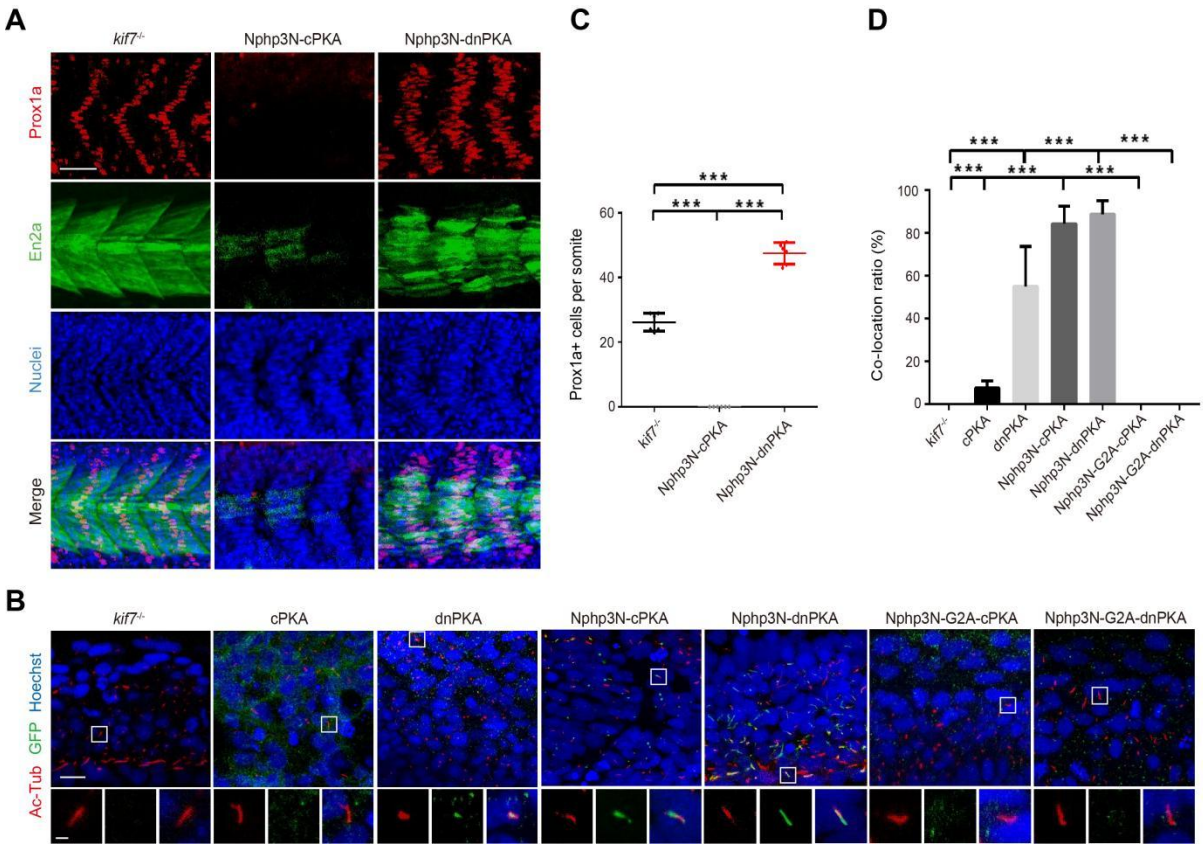

Figure 8. KIF7 did not impede PKA regulation on the HH pathway within the cilia.

(A) The activity of Hh pathway was indicated by expression of Prox1a in red and En2a:eGFP in green in the embryos of *kif7*$^{-/-}$;Tg (*en2a*:*eGFP*)^{sx1005} injected with Nphp3N-cPKA/dnPKA. The nuclei were labelled by Hoechst in blue. Scale bar, 50 μm. (B) Immunofluorescence imaging of *kif7*-null embryos either uninjected or expressing GFP-tagged untargeted cPKA/dnPKA, ciliary cPKA/dnPKA, or extraciliary cPKA/dnPKA. Images depicted 18hpf

somites stained for the GFP tag on cPKA/dnPKA (green), cilia (Ac-Tub, red) and nuclei (Hoechst, blue). Frames indicated cilia depicted in the inset. Insets displayed cilia (left), cPKA/dnPKA alone (middle), overlay of cilia (right). Scale bars, 10 µm and 2.5 µm (inset). (C) Quantification of Prox1a+ cells from experiments presented in A (n = 6 somites in 3 embryos). Unpaired Student's t-test was used for analysis. ns indicates 'not significant' with P>0.05. (D) Quantification of ciliary colocalization from experiments presented in B (n = 60 cilia in 3 embryos). Unpaired Student's t-test was used for analysis, and *** indicates 'significant' with P<0.001.

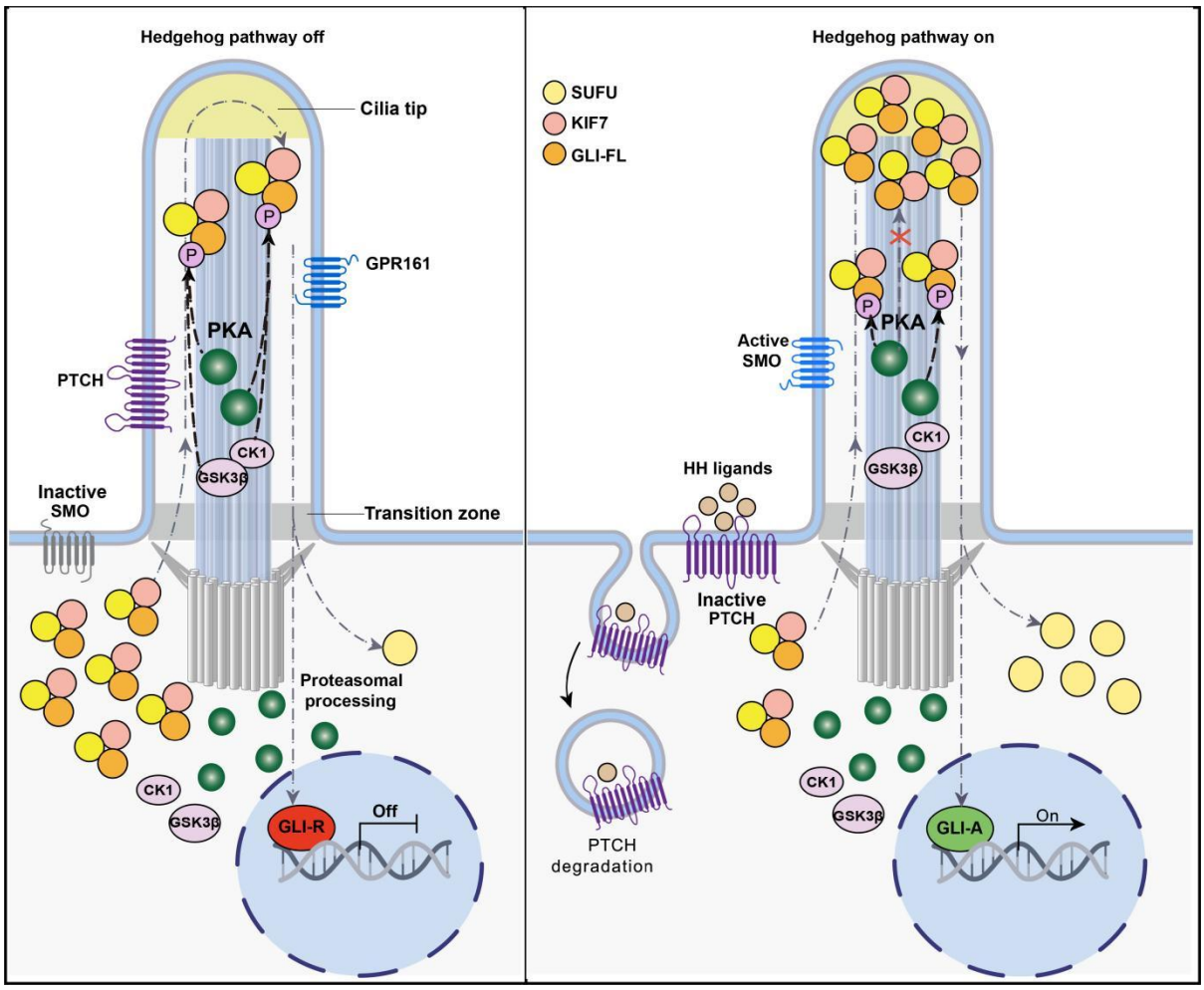

Figure 9. A model for ciliary PKA regulation of downstream transcription factor GLI during HH signal transduction.